THESIS

APPLICATION OF LARGE-SCALE PARTICLE IMAGE VELOCIMETRY TO ENTRANCE FLOWS

Submitted by

Alireza Fakhri

Department of Civil and Environmental Engineering

In partial fulfillment of the requirements

For the Degree of Master of Science

Colorado State University

Fort Collins, Colorado

Spring 2021

Master's Committee:

Advisor: Robert Ettema

Christopher Thornton

Laurel Bond

ABSTRACT

APPLICATION OF LARGE-SCALE PARTICLE IMAGE VELOCIMETRY TO ENTRANCE FLOWS

This thesis presents the findings of application of Large-Scale Image Velocimetry (LSPIV) to illuminate three entrance flows. LSPIV is an image-based method that non-invasively measures two-dimensional instantaneous free-surface velocities of water flow using video equipment. Three different applications used in this study are a flume study with three different contraction ratios, flow through and over spillways in hydraulic models for Gross Dam and Los Vaqueros Dams. For the first application, large-scale-particle velocimetry (LSPIV) was applied to estimate the top-width of the vena contracta formed by an approach open-channel flow entering a contraction of the channel. The experiments investigated the requisite dimensions of two essential LSPIV components: the Search Area and Interrogation Area, to establish the optimum range of these components for use in LSPIV application to contractions of open-channel flows. Of practical concern (e.g., bridge hydraulics) is flow contraction and contraction scour that can occur in the vena contracta region. The thesis showed that optimum values for the Search Area (SA) and Interrogation Area (IA) were 10 and 60 pixels, respectively. Also, the study produced a curve indicating a trend for vena-contracta width narrowing with a variable ratio of approach-channel and contracted-channel widths and varying bed shear stress of approach flow. For the other two applications, the hydraulic models of the spillways for Gross Dam and Los Vaqueros Dam, LSPIV was applied to assess the robustness of LSPIV on mapping the streamlines through and over spillways.

ACKNOWLEDGMENTS

I would like to thank Dr. Robert Ettema for his tireless guidance, and my family for their unlimited support.

TABLE OF CONTENTS

LIST OF SYMBOLS

B1 (m)	The width of the approach channel
B2 (m)	The width of the contracted channel
B2' (m)	The minimum width of the vena contracta
CW	Clear Water
FB	Fixed Bed
FR	Froude number of the uniform approach flow
GRP	Ground Reference Point
IA	Interrogation Area
Kv	Vena Contracta Coefficient
LW	Live Bed
SA	Search Area
SIM	The distance from the top of the search area to the center
SIP	The distance from the bottom of the search area to the center
SJM	Distance from the upstream side of the search area to the center
SJP	The distance from the downstream side of the search area to the center
τ1 (N/m2)	Shear stress
τC (N/m2)	Shear stress for incipient motion

1. INTRODUCTION

1.1 Overview

Large-Scale Particle Image Velocimetry (LSPIV) is an image-based methodology that non-intrusively measures two-dimensional, instantaneous free-surface velocities of water flow using standard, inexpensive video equipment. LSPIV is recognized as a robust means of delineating and quantifying the free-surface flow field [1]. The method has been used on various hydraulic applications, such as flash-flood measurements [2-6], river and stream surface-flow measurements [7-10] and assessing debris-flow velocities in the field [11]. The technique has emerged from Particle Image Velocimetry (PIV), a method used in small flow fields. However, LSPIV uses tracers placed on the surface of flowing water and, by means of a video-camera, tracks the movement of tracers and thereby estimates water-surface velocities. The post-processing data involve using software for digital image-processing, photogrammetry technique, and vector analysis. In this thesis, the open-source software FUDAA- LSPIV [12] is used to implement LSPIV.

FUDAA-LSPIV is an open-source French software developed by EDF and Irstea and is based on previous scientific works on the LSPIV technique. FUDAA-LSPIV was implemented under the GPL license as a user-friendly Java graphical interface that calls Fortran solvers [13]. The version used in this experiment is Version 1.6.2. This version can determine streamlines, flow discharge and can transform images to PNG format without using additional software, making it a very user-friendly software.

The simplicity of the LSPIV method has numerous advantages over other types of velocity measuring techniques, namely Acoustic Doppler Velocimeters (ADV) and Particle Image

Velocimetry (PIV). The use of ADV requires placement of the instruments directly in the flow field, which is cumbersome in big rivers with unsteady flow fields. Moreover, the ADV method only measures velocity at a single point. For instance, in the case of measuring velocity in a wide river, many ADV probes would need to be installed, whereas LSPIV requires the placement of only one camera over the river. Specifically, the LSPIV method has two significant advantages over the PIV method:

1. LSPIV can cover larger flow fields than can PIV, such as flash floods [14];
2. LSPIV uses inexpensive illumination devices and video equipment [14]; and,
3. Another advantage of LSPIV over conventional instruments, such as ADV, is that LSPIV can be used for shallow flows, whereas ADV requires a minimum water depth of 0.25 m [15].

However, LSPIV also has several limitations relating to the equipment (camera, tracer size, and shape) and the nature of the flow field monitored using LSPIV. These limitations have not been thoroughly investigated heretofore.

Flow measurements provide critical information for numerous hydraulic engineering applications related to large water bodies, the dispersion of pollutants in rivers and coastal areas, and problems associated with watershed behavior (erosion, sedimentation, flooding). The LSPIV method has much promise as a reasonably fast way to obtain whole-field measurements of water-surface velocities for free-surface flows. In this thesis, the accuracy and limitations of LSPIV are investigated with regard to determining aspects of flow distribution and the levels of flowrate accuracy. Three different situations were used to reach this goal. The first situation was flow to and through the entrance of a long, contracted channel formed using three different contraction

ratio values, defined in terms of the width of the contracted channel divided with the width of the approach channel, B_2/B_1. The values were B_2/B_1 = 0.25, 0.50, and 0.75. The second situation was flow to and over an ogee crest of a spillway. The third situation was flow to and over a spillway to assess the lateral uniformity of flow distribution. Besides, the flow separation zones over and after the spillway is of interest.

1.2 Objectives

LSPIV is a relatively inexpensive, usually accurate (when suitably applied), and fast method for calculating water-surface velocity. This method has a wide range of applications from small hydraulic lab models to very wide rivers. The accuracy of LSPIV depends heavily on the performance of digital video-cameras used for acquiring a video of flow and on the utility of software for analyzing the video to produce vectors of flow velocities from several assessments of LSPIV accuracy. Compared to other direct measurements of velocity, typical LSPIV error levels were about 3.5% in 1999. Under some problematic flow observation situations, the LSPIV method can still have a 10% level of error. The LSPIV method is continually being improved to refine its accuracy [16]. The accuracy of velocimetry varies on a case-by-case basis and depends highly upon the geometry and particular flow field of interest. Furthermore, in some situations in which the application of LSPIV is difficult, and the results for flow patterns and velocity vectors estimated may have a high level of error.

The overall objective of this thesis was to evaluate the efficacy of the LSPIV method for revealing the water-surface flow fields for the three different, but common, entrance flows mentioned above. This overall objective involved the following specific objectives:

1. Application of the LSPIV technique to three flow-field situations at CSU's Hydraulics Laboratory, to assess the levels of accuracy for water-surface velocity and to map the flow free-surface streamlines for each flow situation;
2. Evaluation of the difficulties and complications associated with each situation and how best to overcome those challenges;
3. Ascertain the sensitivity of, and determining the sensitivity of, the LSPIV parameters Search Area and Interrogation Area for a selected geometry of flow field and the magnitude of velocity. The intent here was to identify the optimum range of parameters to be used in the image-processing step of LSPIV; and,
4. With large-scale-particle velocimetry (LSPIV), estimate the top-width of the vena contracta formed by an approach open-channel flow entering a contraction of a channel. This specific objective is of practical importance for understanding flow through bridge waterways.

1.3 Approach

The experiments involved three different flow fields:

1. Flow through a series of channel contractions with an erodible alluvial bed;
2. Flow to and over an ogee crest of a spillway (Gross Dam Model); and,
3. Flow to and over an ogee crest of an oblique spillway (Los Vaqueros Dam Model).

For this study, an OLYMPUS EM-10 video camera was used for capturing videos, and paper pieces were used as tracers. The diameters of the tracers ranged from 1mm to 20 mm. The paper tracers were produced by simply cutting up sheets of paper to form the larger-size tracers, and a

paper shredder was used for making small-size tracers. Video-camera records were made to capture the particles' displacements on the water surface of the flow by positioning the camera obliquely and above the interest area. The LSPIV software was then used to analyze the resulting images of flow and produce free-surface velocity vectors. The velocity vectors could then be directly assembled to form two-dimensional vector fields of the surface of the flow observed [16].

2. BACKGROUND AND THEORY

2.1 Introduction

This chapter compares several velocimetry methods that could be used as an alternative to LSPIV. Along with LSPIV, the following techniques are discussed, with an analysis of their respective advantages and disadvantages:

- Particle Image Velocimetry (PIV)
- Acoustic Doppler Velocimetry (ADV) probes
- Pitot tubes

2.2 PIV

PIV is an optics-based method that determines velocity fields by measuring particle-tracer displacements within the flow region. For the successful application of PIV, the following elements are required:

- Illumination source – to make the tracer particles readily visible
- Digital video-camera – to record the motion of the tracer particles
- Electronics – to synchronize the camera and light source
- Software package – to analyze the digital images and calculate the velocities of the tracer particles [14].

PIV is a useful method of velocimetry because it is quick and nonintrusive. This method readily yields estimates of the mean velocity flow field and gives higher-order moments of the velocity

probability distribution over large spatial domains. PIV also can be used to calculate two-dimensional instantaneous flow velocity vectors (magnitude and direction) and two-dimensional continuous velocity distributions [16], doing so over the depth of a flow.

Despite PIV's robustness, it is not without drawbacks. Namely, PIV requires clear-water discharge and naturally buoyant tracer particles, which may be lost in the flow. Moreover, it can be challenging to set up a PIV configuration. PIV is most adequately implemented in a very clean laboratory setting, wherein the range of possible flow fields is limited; PIV is not well suited for large scale situations such as flood flows in river channels and or coastal currents occurring in coastal settings.

2.3 LSPIV

Within the past three decades, developments in optics, lasers, electronics, and computer-related technologies have made the visual investigation of flow fields more possible. LSPIV, a technique derived from PIV, is a handy method for calculating water-surface velocities and mapping the flow pattern at large scales such as flood flows. The obtainment of 2-dimensional velocity fields at the water-surface is made possible with frame-by-frame analysis of the tracer particles to yield their time-relative displacements. Typical tracer particles include paper clippings, debris, small floats, etc. The main principles of LSPIV include the following considerations:

- Recording images with a known time step (Δt)
- Applying orthorectification – a geometric correction to the images to fix the perspective distortion
- Measuring the displacement of tracers and calculating the water-surface velocities.

LSPIV applies a cross-correlation statistical method on the orthorectified images to measure the tracer particles' spatial displacements. The two critical parameters for calculating tracer velocities are the Interrogation Area (IA) and Searching Area (SA). Both parameters are discussed in greater detail in the upcoming chapters of this thesis.

Although LSPIV is generally recognized as fast, inexpensive, and reliable, its accuracy in specific contexts is questionable, e.g., in measuring flow fields through contractions, near boundaries, and in regions with high-velocity gradients. In the present thesis, the application of LSPIV to these contexts is investigated. Additionally, LSPIV may not be accurate for flow fields involving significant vertical (non-planar) components of velocity or when the water surface is wavy.

2.4 Pitot Tube and Acoustic Methods

The Pitot tube and acoustic method, notably the acoustic-Doppler velocimeter (ADV), are intrusive devices that measure flow velocity at a point within a flow. Consequently, they can be laborious to use when attempting to map an entire flow field. Contrary to the previously discussed optical methods, the Pitot tube and ADV may affect the local flow direction or velocity magnitude by their intrusive nature. Each device yields velocity measurements at a point, and therefore, neither is well suited for analyzing large areas of flow; e.g., wide-river flows.

The Pitot tube is the most straightforward method of measuring flow velocity magnitude, though it yields only velocity magnitude and not velocity direction and can be inadequate for measuring turbulence. A Pitot tube operates by the pressure difference between a local ambient pressure head and the pressure head generated at a stagnation point in the flow, as basic texts on

fluid mechanics describe. The pressure head comprises two components: the local pressure and the dynamic pressure associated with the water's motion. By subtracting the local (ambient) pressure from the total pressure, the dynamic pressure is obtained and used to calculate the flow velocity.

Acoustic Doppler Velocimetry measures the Doppler frequency shift to determine the velocity and flow direction. After emitting acoustic waves into the flow, the waves are scattered by water particles. When this scattering occurs, the Doppler Effect occurs; i.e., the frequency or wavelength of the acoustic waves seems to change for an observer who is moving relative to the wave propagation. To obtain the flow velocity from this Doppler Effect, ADV uses a transmitter and receiver to determine the waves' travel times.

3. APPLICATION OF THE LSPIV METHOD

3.1 Introduction

This chapter describes the experiments and their arrangements as used in the applications this thesis describes. In this chapter, two different situations are investigated to measure the accuracy of the LSPIV method and the fields in which LSPIV has the most accurate results. The first situation is flow through the three different contractions (0.25, 0.5, and 0.75). This experiment's motivation was to determine water-surface velocities around the different contraction ratios over an erodible sand bed. Also, in this chapter, the capability of the LSPIV method and its precision to determine flow fields and estimating the vena contracta are investigated.

Further, this chapter describes the methods that were used to determine the optimal values of the LSPIV parameters. Selecting the optimal values of the LSPIV parameters comprises a critical step in using the LSPIV method and, thereby, produces accurate results. Thus, the Fudaa LSPIV parameters had first to be correctly determined. In this regard, the two crucial parameters in LSPIV are Interrogation Area (IA) and Search Area (SA). The Interrogation area must be large enough to incorporate tracers but small enough to represent the flow (velocity gradients in an IA must be negligible). The SA is a rectangle defined around the center of the IA, and SA corresponds to the zone in which the patterns are searched on the successive images. Setting these parameters are discussed further in this chapter.

3.2 Vena Contracta in Open-Channel Flow

A vena contracta develops when flow narrows and separates from the flow’s boundaries as it passes into a contracted area of flow. In free-surface flows, vena contracta formations are often reported for flows entering spillways and outlets, e.g., for free- and submerged-flow discharges

through ungated and gated spillways [17, 18]. For example, previous studies included investigations of a vena contracta formed when flow passed beneath sluice or spillway gates [19]. Vena contracta formations often occur within reservoir spillway flows [20] and for flow along pressurized conduits with geometry changes [21]. The width and depth of vena contracta formations were measured with different methodologies, e.g., dye tracers and dye injections [22, 23], and Particle Tracking Velocimetry (PTV) [24]. However, a substantial gap in the literature [25] exists regarding vena-contracta formation within a contraction entrance of open channels and how the dimensions of such vena contractas vary with channel geometry and flow conditions. This gap has significance for understanding flow through bridge waterways. LSPIV is a seemingly convenient method to gain information on the top-width of a vena contracta formed by an approach open-channel flow entering a contraction of the channel. Moreover, it is more convenient than alternative methods like ADV measurements or dye as it is readily applicable, provided suitable magnitudes of IA and SA are selected to facilitate LSPIV accuracy.

3.3 Experiments

As mentioned in Chapter 1, three different situations were used in this study. The following flow situations were used in this study:

3.3.1 The 2.4-meter flume

Figure 3.1(a) shows a photograph of the 2.4 m-wide flume. This flume is located at Engineering Research Center at Colorado State University. Figure 3.1(b) shows a schematic of the dimensions of this flume. The flume was set up to investigate contraction scour for three different contraction ratios, B_2/B_1. There are three discharge lines to supply water to this flume. In this study, Pump

No.2 was used to provide the required range of flows. This pump is capable of delivering 0.453 m^3/s discharge to the flume's test channel.

Figure 3.1. Views of the flume: (a) A view of the 2.4-meter flume; and, (b) a schematic view of the flume

Two sidewalls were installed for making the contractions of variable B_2/B_1. Three different ratios were used for this study: tight (B_2/B_1 = 0.25); medium (B_2/B_1 = 0.5); and, modest, (B_2/B_1 = 0.75). Figure 3.2 shows a schematic of the 2.4 m-wide flume and the experimental setup used for this flume. Figure 3.3 shows the approach of the flume. The approach channel was 9.14 m long and contracted to a 25.9 m long narrowed channel. This flume can provide the bed slope in a range of horizontal and a maximum slope of 2 percent. Figure 3.4 shows the three different ratios that were used in this flume.

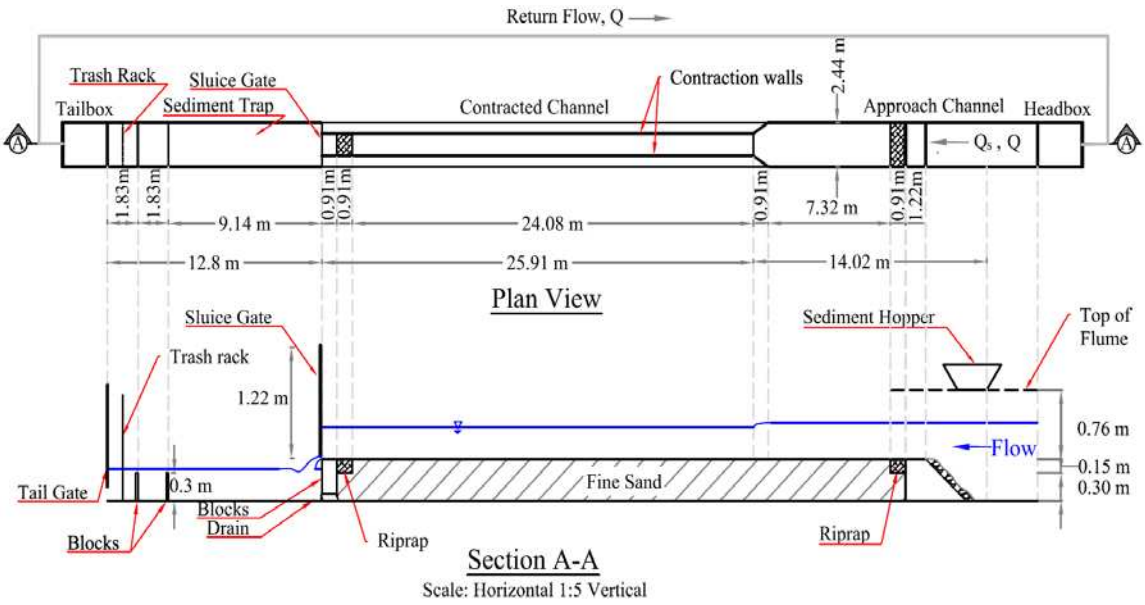

Figure 3.2. Overview of flume setup used for the contraction scour experiments

Figure 3.3. A view of the approach for B_2/B_1= 0.25

(a) (b) (c)

Figure 3.4. Views of the contracted flume for three different contraction ratios:(a) B_2/B_1=0.25;(b) B_2/B_1=0.50; and, (c) B_2/B_1=0.75

As mentioned above, this flume's setup was designed mainly for enabling measurement of the scour depths along the bed of contracted channels subject to three values of B_2/B_1. For this purpose, fine sand was used to cover the bed with a depth of 0.457 m. A platform was made on the flume for setting up the camera, and Figure 3.5 shows the platform used for locating the camera.

Figure 3.5. The platform used for the camera setup

For the scour study on this flume, a combination of 31 different discharges and situations were tested, and 19 experiments out of 31 runs were selected for the LSPIV investigation. Table 3.1 indicates the operations used for LSPIV, and also it includes information about the corresponding discharge and ratio for each particular experiment. The scour study on this flume consists of three different conditions, Live Bed (LB), Clear Water (CW), and Fixed Bed (CW-Fixed) which are indicated in the test names in Table 3.1.

Table 3-1. Test numbers and their corresponding discharge (Q) and contraction ratio (B_2/B_1)

Test Condition	**Contraction Ratio (B_2/B_1)**	**Discharge Q** (CMS)
LB	0.75	0.190
LB	0.75	0.231
CW	0.75	0.111
LB	0.75	0.161
LB	0.75	0.138
LB	0.75	0.288
CW	0.75	0.099
CW	0.25	0.064
CW	0.25	0.087
LB	0.5	0.231
LB	0.5	0.161
LB	0.5	0.190
LB	0.5	0.138
CW	0.5	0.064
CW	0.5	0.076
CW	0.5	0.087
FB	0.25	0.064
FB	0.25	0.092
FB	0.25	0.076

In this study, two sizes of paper tracers were used. Figure 3.6 depicts the two sizes. All the tracers were made from regular printing paper that was easy to observe by the video camera. For the seeding part of each experiment, an adequate number of particles were placed (sprinkled upstream of the experiment location) to provide enough tracer coverage for at least fifteen seconds of video-recording and to adequately cover the whole flow field of interest. This step took careful timing in terms of applying the tracers and readying the video camera.

Figure 3.6. The two different sizes of tracer particles used (all formed from paper)

3.3.2 The Gross Dam Model

Figure 3.7 shows two views of the hydraulic model of the new, stepped spillway for the heightened Gross Dam. The need for the spillway arose as part of the Gross Dam Expansion (GRE) Project, which raises the existing Gross Dam by about 40.0 m to an ultimate height of 143.6 m. This model was built at a length scale of 1:24 in the Engineering Research Center (ERC) at

Colorado State University. The purpose of the model was to evaluate the characteristics of flow aeration and energy dissipation along a large-scale stepped chute of unique geometry. Figure 3.8 shows a profile view of the Gross Dam, and Figure 3.9 shows a plan view of this model.

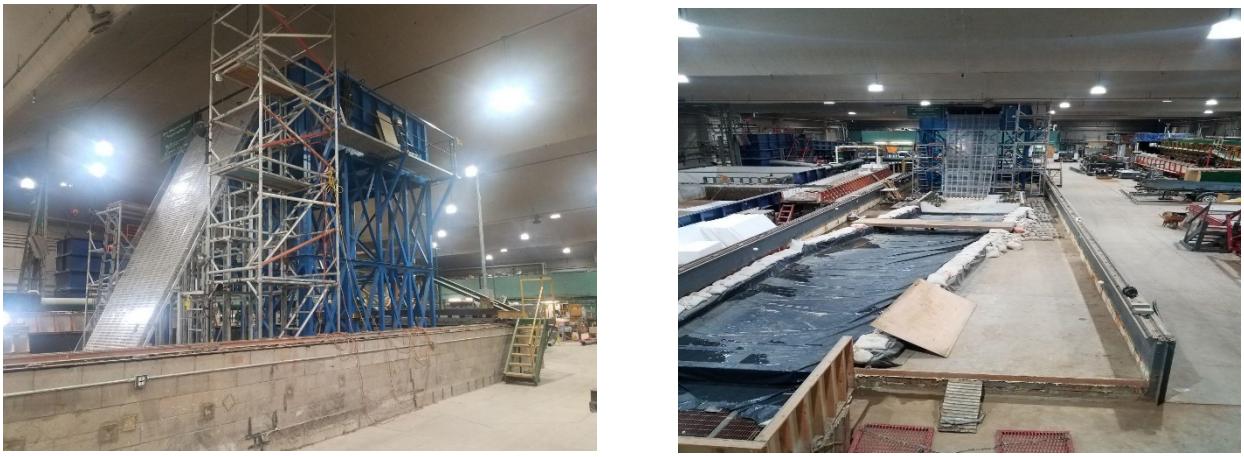

Figure 3.7. Two views of the hydraulic model under construction of the spillway for Gross Dam

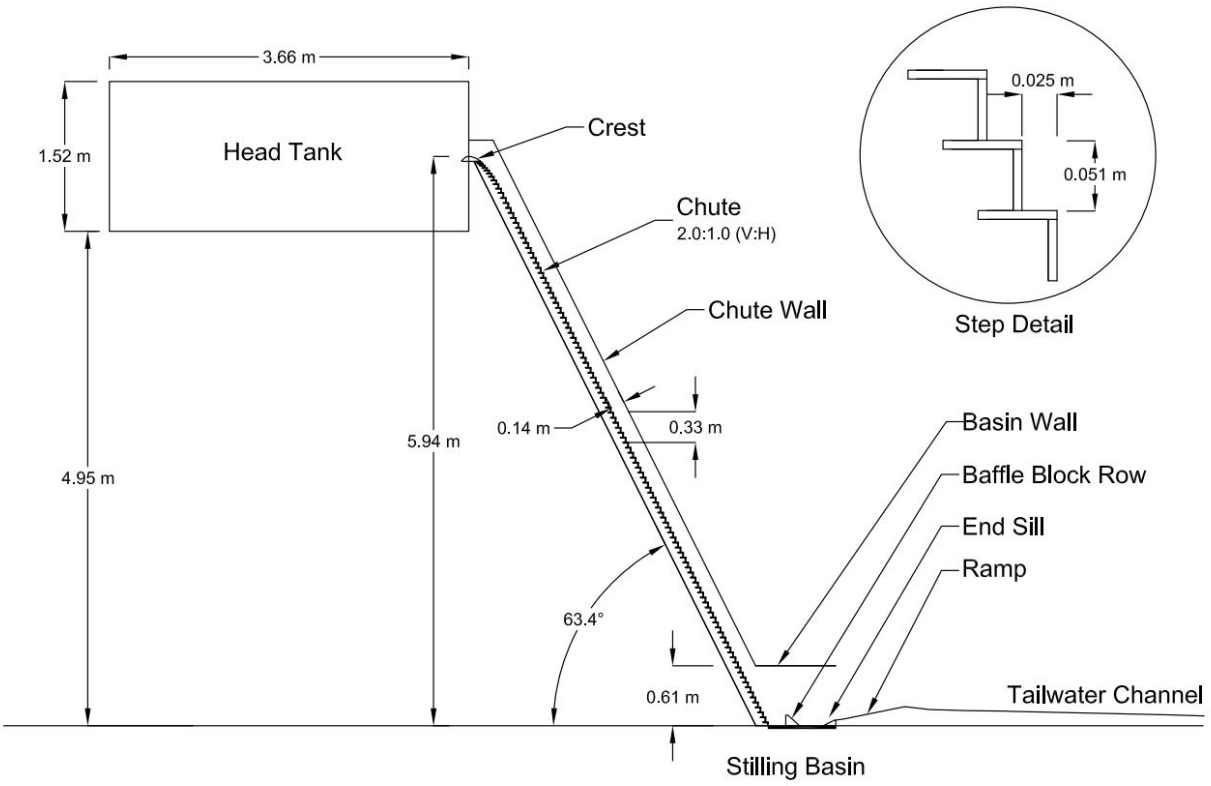

Figure 3.8. A profile view of the spillway for Gross Dam

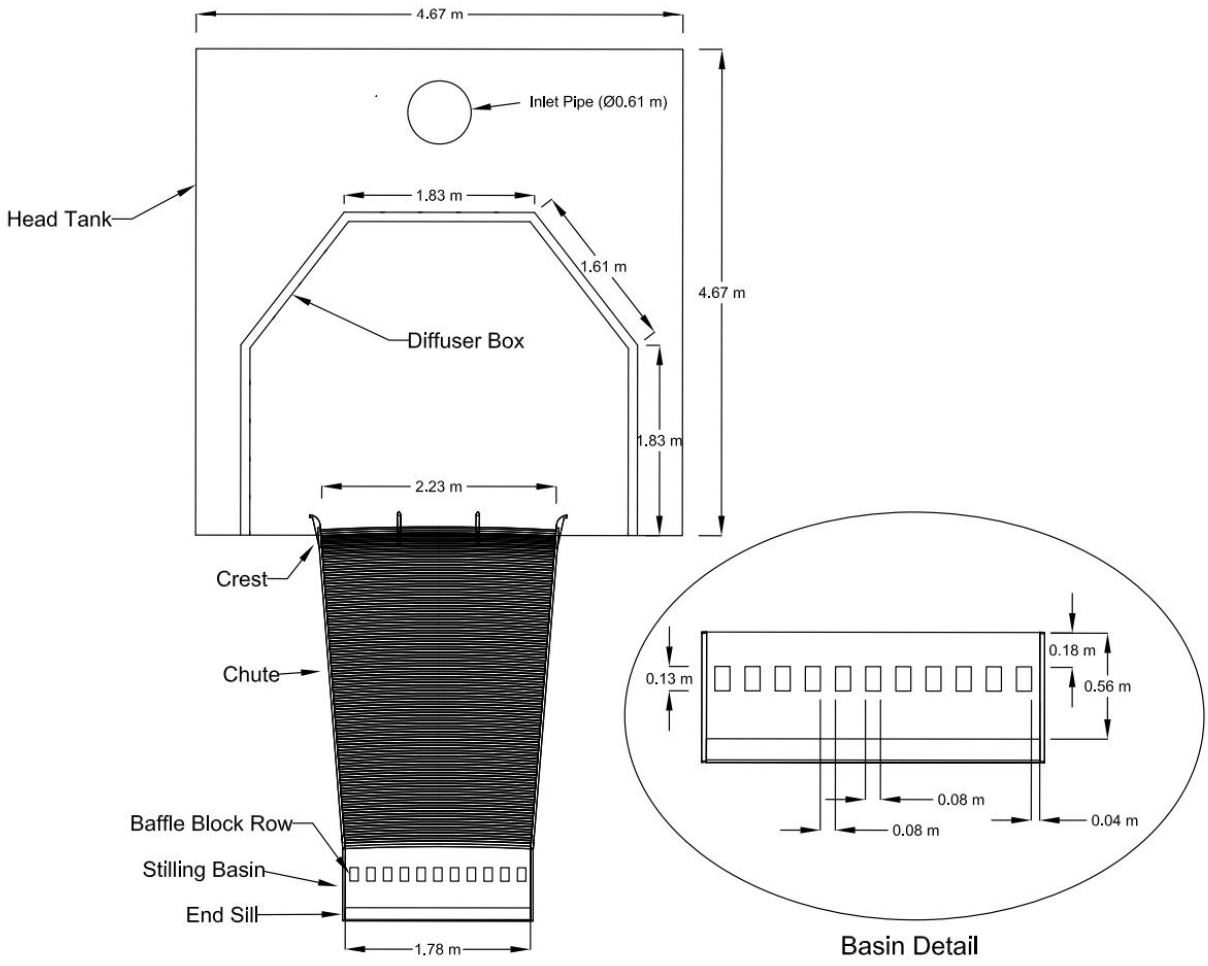

Figure 3.9. A plan view of the spillway for Gross Dam

Some critical components of the model include the following items:

- The head tank, whose plan dimensions were 4.67 m by 4.67 m and a depth of 1.52 m. The tank had a diffuser box to provide a uniform flow through the ogee crest. The diffuser box was made of multiple layers of semi-permeable mesh.
- The crest, which was formed as an ogee-crest shape. Two piers were installed at 1/3 and 2/3 of the length of the crest
- The design discharge is 0.347 m^3/s

In this study, the lateral uniformity of flow distribution to and over the ogee crest was of interest, especially for evaluating the spillway's performance. The flow over an ogee crest had a 3D flow pattern, with flow converging toward the crest, flow upwelling from the reservoir, and flow accelerating over the crest and then down the spillway. Accordingly, this model was useful for determining the capability of the LSPIV technique for spillway-crest flows. Two paper sizes were used for seeding the flow, and the dimensions of each were the same as for the 2.4-meter flume.

3.2.3 The Los Vaqueros Dam Model

The Los Vaqueros Reservoir Expansion (LVRE) Project is located on Kellogg Creek near Brentwood, California. The objective of the Los Vaqueros Reservoir Expansion project is to raise the existing Los Vaqueros Dam by 17.7 meters, increasing storage capacity from approximately 197.4 million cubic meters to about 339.2 million cubic meters.

The layout of the simulated reservoir was constructed in a space that encompassed a 41.83 m-wide, 34.67 m-long by 10.67 m-deep volume of Los Vaqueros Reservoir adjoining and centered on the location of the new spillway in addition to a space that encompasses a 16.38 m-wide, 16.38 m-long by 17.68 m-deep volume centered over the sluice intake. A 40 hp (30 kW) pump was used to deliver the flow through an 0.46-meter diameter pipe, into two 0.2-meter diameter pipes, which led to both head tanks of the model, and the flow rate through the model was 0.17 m^3/s (PMF). Figure 3.10 shows the isometric of the model, and Figure 3.11 shows the model's overhead photo.

In this study, the lateral uniformity of flow distribution to and over the spillway is investigated. Besides, the flow separation zones over and after the spillway are of interest.

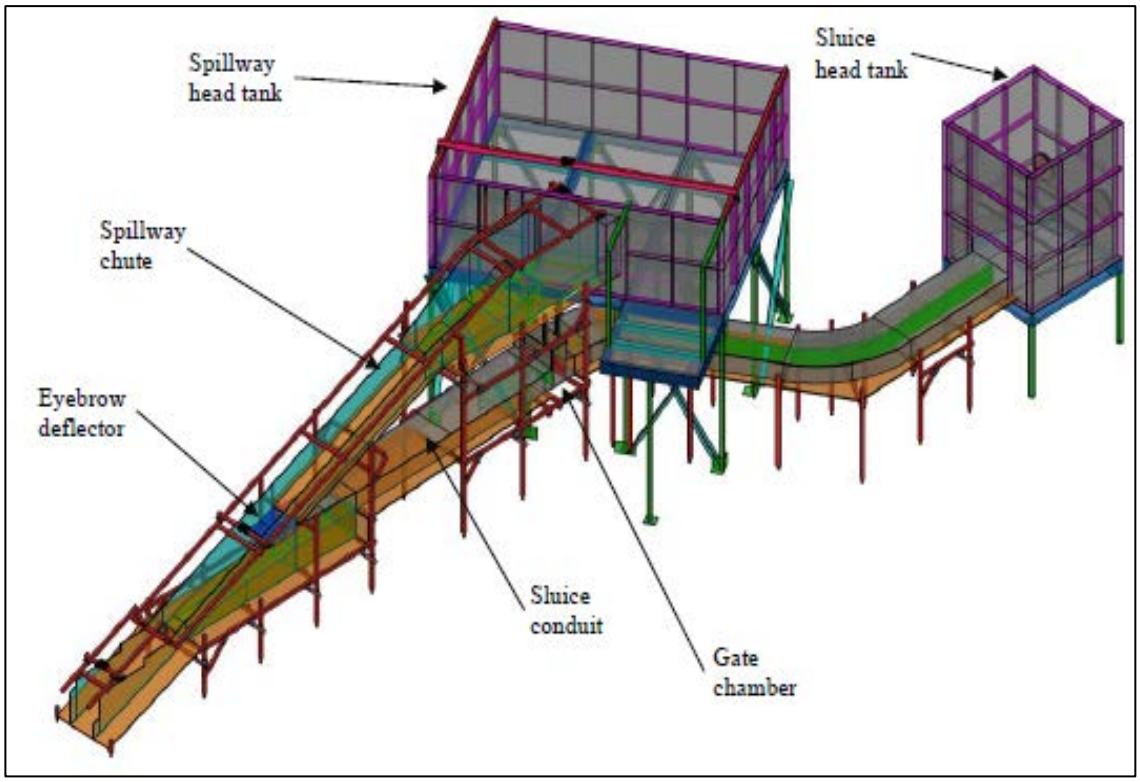

Figure 3.10. Isometric view of the model of Los Vaqueros Dam

Figure 3.11. Overhead photo of the model of Los Vaqueros Dam

3.4 LSPIV Software

3.4.1 Approach

In this study, the software Fudaa (https://forge.irstea.fr/projects/fudaa-lspiv) was used to convert video images and calculate velocity vectors. The version used was Version 1.6.1. This version has the capability of calculating streamlines, flow discharge, and transforming images to PNG form without using any additional software, thereby making it a more user-friendly version than earlier versions.

A requirement for suitably accurate LSPIV is the acquisition of a detailed video image. An OLYMPUS EM-10 video camera was used for this task. The camera had a 4k format, such that the resulting images had a maximum size of 3840×2160 pixels recorded at a rate of 30 images per second (fps). The area of interest should cover all benchmarks. Also, it was essential to avoid any vibration and reflection. To avoid these problems, the camera was set on a tripod, and the possibility of reflection from the water surface was checked to be absent.

Paper pieces were used as tracers, and their sizes range from 1mm to 20 mm. Paper pieces, produced by simply cutting up a sheet of paper for big-sized tracers and a paper shredder were used to make small size tracers. Video-camera records were recorded to capture the displacements of the particles on the water surface of the flow by positioning the camera obliquely and vertically to the interest area. The LSPIV software was then used on those images of flow and provided free surface velocity by producing two-dimensional vector fields of flow.

The LSPIV technique calculated the movement of paper tracers on the water surface flow to and within the contraction entrance. Most of the applications were made for the 2.4-meter flume

once the contraction scour had attained an equilibrium condition. The Fudaa software involved the following steps in calculating flow velocities:

1. Begin the software setup and select the video-record the resulting image of tracer movements;
2. Orthorectify the images and define each benchmark location;
3. Define an interrogation area and a search area;
4. Form the estimation grid; and,
5. Calculate the local velocity values at each position and then determine the average values of velocity at each position.

The ensuing sub-sections of this thesis elaborate each of these steps.

3.4.2 Benchmark Setup

The LSPIV techniques required the use of a system of benchmarks to locate the flow and enable orthorectification of the video image, which had to be taken at an oblique angle because of head-space limitations. The Fudaa-LSPIV offered two methods of orthorectification:

- Scaling: When images are not distorted by perspective effects (vertical viewpoint), easy scaling is sufficient for the software to determine dimensions
- Complete Orthorectification (2D, 3D): When perspective effects distort images, a complete orthorectification is needed based on reference points

Figure 3.12 shows the three ways of orthorectification in Fudaa-LSPIV software. In this study, complete orthorectification was used to define the benchmarks because of not having access to the roof to install the camera perpendicularly above the flume

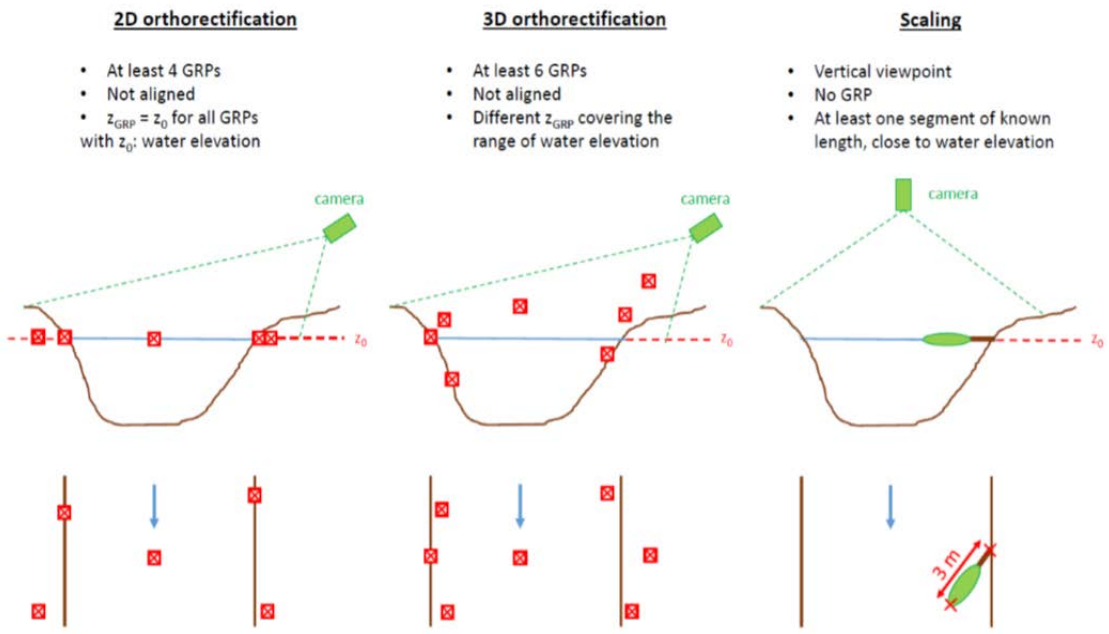

Figure 3.12. The methods used for orthorectification of images processed in the Fudaa-LSPIV software

3.4.2.1 The 2.4-meter Flume

Figure 3.13 shows the benchmarks and their locations that were selected for the 2.4-meter flume. Table 3.1 gives the corresponding coordinates of the benchmarks for the three different contraction ratios. This table uses metric units (meters), and the errors are noted in the Gap column.

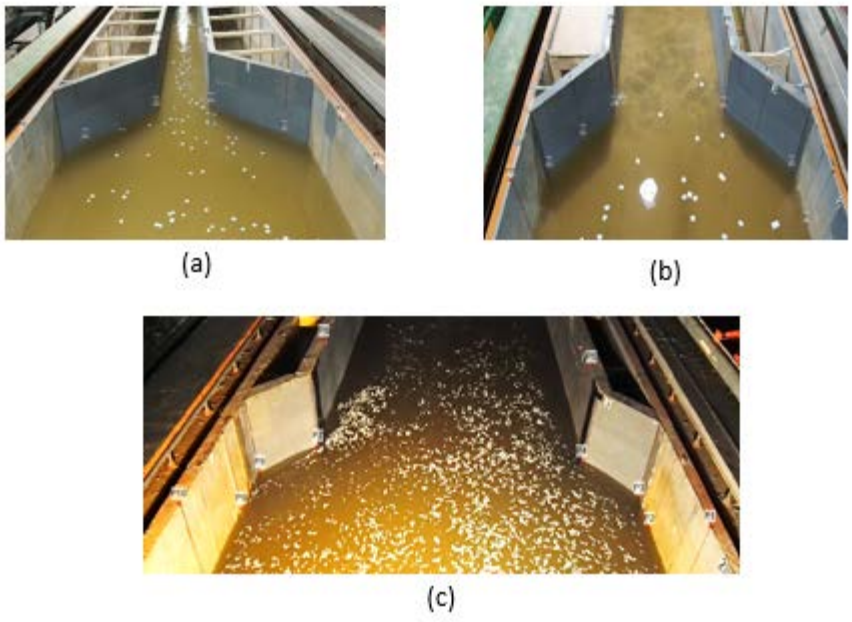

Figure 3.13. LSPIV tracers entering the contracted channel: (a) benchmark locations for the 0.25 ratio contraction; (b) benchmark locations for the 0.5 ratio contraction; and, (c) benchmark locations for the 0.75 ratio contraction

Table 3-2 Benchmark coordinates: (a) benchmark coordinates for the 0.25 ratio contraction; (b) Benchmark coordinates for the 0.5 ratio contraction; and (c) benchmark coordinates for the 0.75 ratio contraction

(a)

#	Real X	Real Y	Recalculated X	Recalculated Y	Gap
1	0.000	0.000	0.012	-0.007	0.014
2	0.610	0.000	0.604	0.006	0.009
3	1.524	0.178	1.513	0.174	0.012
4	2.225	0.876	2.230	0.888	0.013
5	2.744	0.914	2.746	0.912	0.003
6	2.744	1.524	2.751	1.523	0.007
7	2.225	1.562	2.215	1.556	0.012
8	1.524	2.260	1.541	2.263	0.017
9	0.610	2.438	0.596	2.434	0.015

(b)

#	Real X	Real Y	Recalculated X	Recalculated Y	Gap
1	0.000	0.000	0.004	-0.002	0.005
2	0.483	0.000	0.476	0.002	0.007
3	0.788	0.305	0.805	0.305	0.018
4	1.093	0.610	1.080	0.604	0.014
5	1.397	0.610	1.389	0.611	0.008
6	1.397	1.830	1.400	1.824	0.006
7	1.093	1.830	1.097	1.841	0.012
8	0.788	2.135	0.789	2.141	0.006
9	0.483	2.440	0.491	2.432	0.011
10	0.000	2.440	-0.011	2.438	0.011

(c)

#	Real X	Real Y	Recalculated X	Recalculated Y	Gap
1	0.000	0.000	0.004	-0.002	0.005
2	0.483	0.000	0.476	0.002	0.007
3	0.788	0.305	0.805	0.305	0.018
4	1.093	0.610	1.080	0.604	0.014
5	1.397	0.610	1.389	0.611	0.008
6	1.397	1.830	1.400	1.824	0.006
7	1.093	1.830	1.097	1.841	0.012
8	0.788	2.135	0.789	2.141	0.006
9	0.483	2.440	0.491	2.432	0.011
10	0.000	2.440	-0.011	2.438	0.011

3.4.2.2 Gross Dam

Figure 3.14 shows a view of the head tank with benchmarks and their selected locations. The pink dots shown in this picture indicate the desired areas for benchmarks. The flow near and over the crest has a variable flow depth that makes it hard to install permanent benchmarks. Also, to get accurate results with the Fudaa-LSPIV software, benchmarks are needed to encompass the water level's perimeter. Thus, it was devised to implement a measurement scale in each benchmark. Later, before each experiment, a photo was taken of the benchmarks, and then the accurate water

level was assessed for use in the Fudaa-LSPIV. Figure 3.15 shows the benchmarks and the measurement scale during one of the tests, and Table 3.3 indicates their corresponding coordinates.

Figure 3.14. The benchmark locations used in the hydraulic model of Gross Dam (The pink dots indicate benchmark locations)

Figure 3.15. The measurement scale and benchmarks for the hydraulic model of the reservoir approach to Gross Dam spillway

Table 3-3 The coordinates of benchmarks for the Gross Dam model

#	Real X	Real Y	Recalculated X	Recalculated Y	Gap
1	0.000	0.000	-0.001	0.002	0.003
2	0.361	0.000	0.366	-0.007	0.009
3	0.762	0.000	0.760	0.002	0.003
4	0.762	0.406	0.759	0.411	0.005
5	0.762	1.245	0.759	1.245	0.003
6	1.067	1.245	1.072	1.244	0.005

3.4.2.3 Los Vaqueros Dam Model

For the Vaqueros Dam model, seven benchmarks were selected. Figure 3.16 shows the selected benchmarks and their locations.

Figure 3.16 The benchmark locations used in the hydraulic model of Los Vaqueros Dam

Table 3-4 The coordinates of benchmarks for the Vaqueros Dam model

#	Real X	Real Y	Recalculated...	Recalculated...	Gap
1	0.000	0.000	0.022	-0.012	0.025
2	0.005	0.334	0.000	0.342	0.010
3	0.196	0.580	0.178	0.579	0.018
4	0.425	0.619	0.381	0.623	0.044
5	1.237	0.604	1.262	0.604	0.025
6	1.250	1.290	1.232	1.287	0.018
7	0.437	1.305	0.477	1.308	0.040

3.4.3 Select Images

The first step for using the LSPIV software entailed selecting a sequence of images in a video record (video). The video was uploaded in the software, and the beginning and the end of the video were then defined. For all the measurements, the number of frames per second was kept at 30 fps. The number of images used for each measured varied from 200 to 500 to find the best interval for which the paper tracers covered the entire flow field associated with flow passing through a vena contracta and the crest. Further, the tracers had to be easy to see for every image and not be contaminated with other influences, such as intermittent light reflections off the water surface.

3.4.4 Orthorectification

In this step, every point in the images was related in position to the positions of the benchmarks, because every point in each image had to be the same in the whole sequence of images. This step was quite vital for the orthorectification process. However, it was theoretically possible to change the data on points in the images to ensure that the process is correctly implemented and proceeds accurately; position adjustment was not used for this study.

To get a suitably correct orthorectification of an image took the use of a minimum of six benchmark locations. These locations needed to be reasonably uniformly distributed in the image. It then was possible to define the transformation parameter and use the software to calculate default values. The water-surface level variation was related to the benchmark locations. The next step entailed transforming all images based on the input data and calculating the velocities. As the last

step, after orthorectification, the benchmark locations in each image were checked. A risk was that an image could be stretched or shrunk or may be blurry after the orthorectification process.

Figure 3.17 shows the orthorectified image for one of the 2.4-meter flume experiments with B_2/B_1 = 0.5, and Figure 3.18 shows the orthorectified image for the Gross Dam experiment. For Los Vaqueros Dam model, see Figure 3.16.

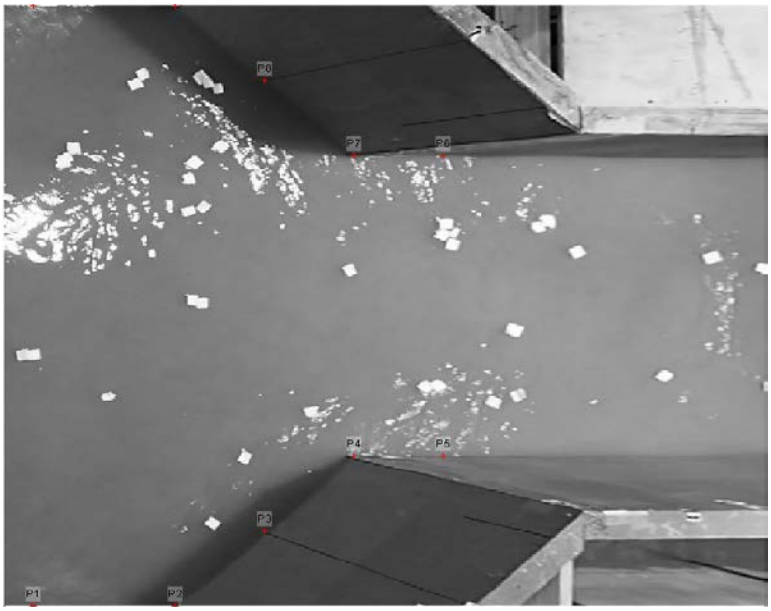

Figure 3.17. The orthorectified image of the contraction entrance used when B_2/B_1=0.5

Figure 3.18.10 The orthorectified image for the experiment done at the entrance to Gross Dam spillway

3.4.5 Interrogation Area and Search Area

The interrogation area (IA) was a square area that incorporates all the tracer particles and represented the scales of interest within the vena-contracta flow field. The area was not so large that the IA adversely affected the calculation efficiency. Yet, it was not so small that it made the results insufficiently accurate.

The search area (SA) is a rectangle with the same center as the IA. It is an area that shows the essential flow patterns on a set of continuous images. The SA can be extended in dimension to ensure the results are suitably accurate for the study. The SA was defined using four direction

variables: Sim, Sip, Sjm, and Sjp. Figure 3.19 shows these four parameters. The brief definition of variables is as follows:

Sim = the distance from the top of the search area to the center.

Sip = the distance from the bottom of the search area to the center.

Sjm = distance from the upstream side of the search area to the center.

Sjp = the distance from the downstream side of the search area to the center.

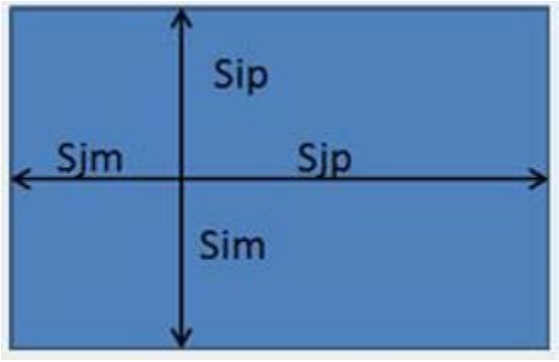

Figure 3.19. Sim, Sip, Sjm, and Sjp

One run from the modest contraction ratio (B_2/B_1 = 0.75) was selected to find the best values for IA and SA. This experiment had a discharge of 0.138 m^3/s, and the flow depth was 21.0 cm at the approach cross-section. To estimate the most accurate value for IA, Sim, Sip, Sjm, and Sjp were kept at 10 pixels initially as Sutarto (2015) mentioned the best value of Sim to be 7 pixels for waterways with expansions [26]. Then, the IA's assumed different values; i.e., 90, 80, 60, 50, 40, 30, and 20, were assigned to measure the magnitude of velocity vectors. For comparing the accuracy of results, velocity vectors were measured by ADV at 28 points over the interest area.

These points were selected to cover the whole flow field, including approach, near walls, and the contracted area. Figure 3.20 shows the selected points and their locations. The findings from LSPIV were then compared with the ADV results to find the most accurate value for IA. In the next step, the best value of IA was kept constant, and the SA components were selected, e.g., Sim, Sip, Sjm, and Sjp = 5, and 15. Finally, values of IA and SA having the minimum error were used for the rest of the experiments.

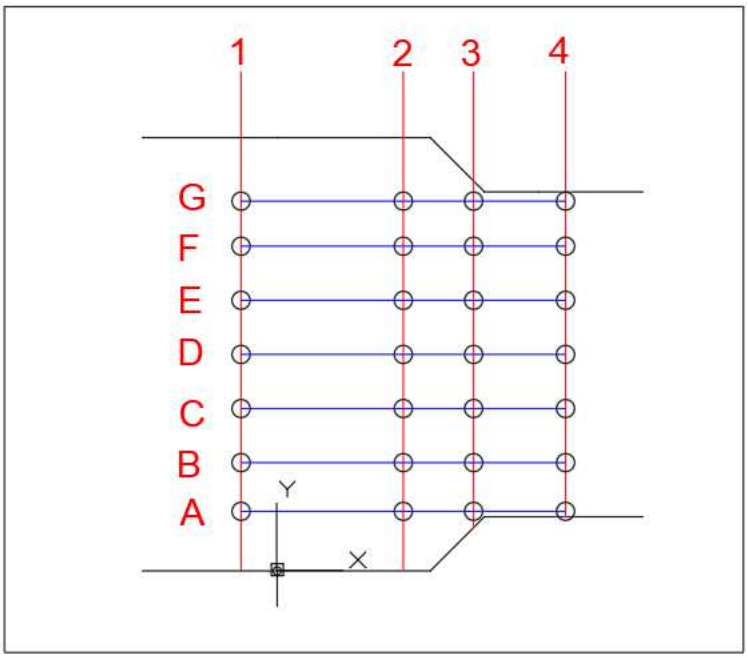

Figure 3.20. Selected points for the ADV data collection

For each set of data collection by means of the ADV, the flow depth was measured using an acoustic sensor, and the velocities were collected at 0.6 of the flow depths. The velocity at 0.6 flow depth gives the average velocity and estimates the surface velocities by ADV, and it was assumed that the mean velocity in a vertical profile is 80-90% of the water surface velocity [27]. Then, all the ADV data were adjusted to compare with the LSPIV findings. The measured free-surface

velocities with a basic LSPIV system have uncertainties ranging between 10% and 35% (at 95% confidence level) [14]. In this study, 15% precision was selected as the acceptable level of accuracy to compare ADV and LSPIV measurements. The results have shown that the best values for IA and SA are 60 pixels and 10 pixels [28], respectively, and discussed in the next chapter.

3.4.6 Defining the Grid

A grid setup was used to define the position of the points for data measurement. The grid size was defined using the research area and the test target of interest. It should be noted that using minimal grid size significantly increased the time needed for velocity calculation. In this study, for the 2.4-meter flume, the number of grids was selected 30 by 30, and for the Gross Dam experiment, the number of grids was selected 20 by 25. Figure 3.21 shows the grid setup used for the 2.4-meter flume when $B_2/B_1 = 0.5$, and Figures 3.22 and 3.23 show the grid setup for the Gross Dam and the Los Vaqueros Dam models, respectively.

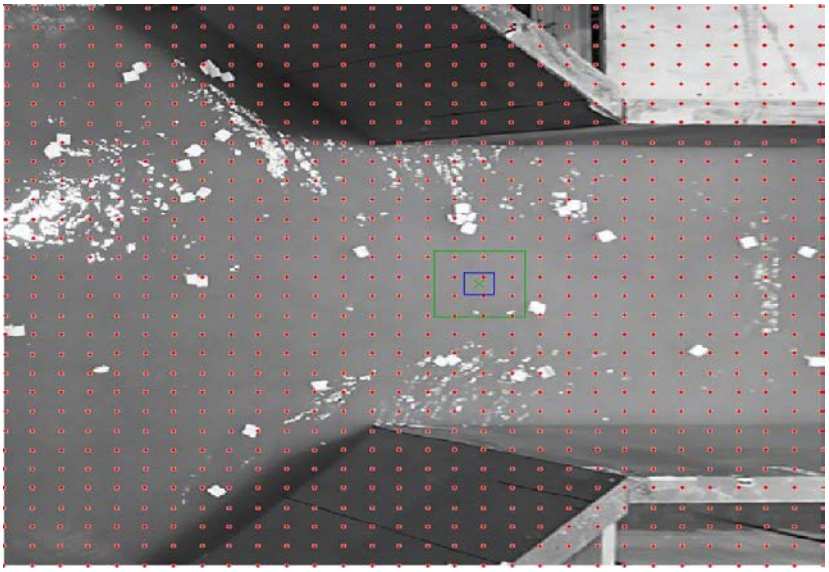

Figure 3.21. Delineation of the grid for the 2.4-meter flume, and the red points as the measurement points

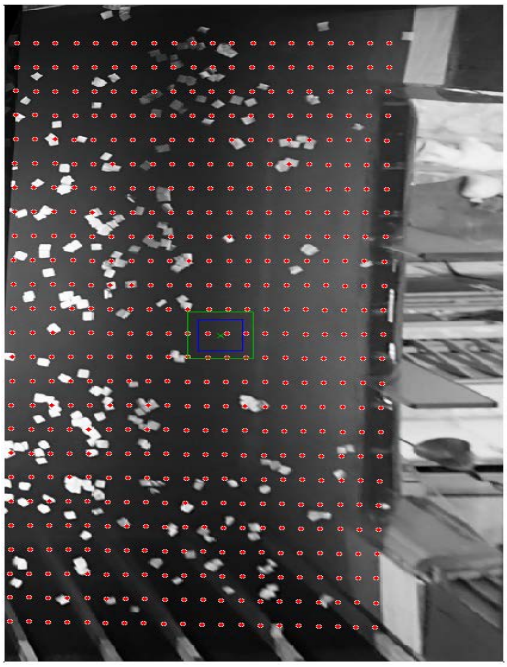

Figure 3.22. Delineation of the grid for the entrance to the model spillway for Gross Dam and the red points used as the measurement points

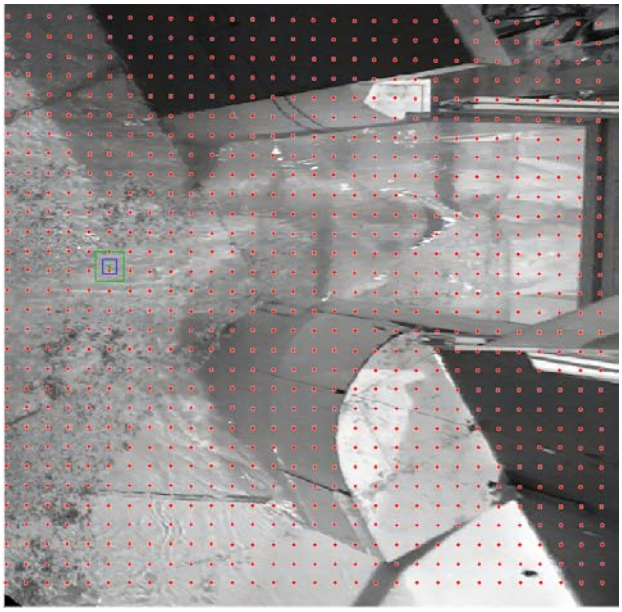

Figure 3.23. Delineation of the grid for the entrance to the model spillway of Los Vaqueros Dam and the red points used as the measurement points

3.4.7 Estimation of Local Velocities

After setting up all the Fudaa LSPIV software variables, the software was used to estimate instantaneous values of water-surface velocity. These values were then used to calculate the average water-surface velocities and streamlines at the measurement location. Figure 3.24 shows the instantaneous vector velocities estimated using the Fudaa LSPIV for the 2.4-meter flume. Note that the velocities in this figure are for a single step and include errant values (to be removed by filtering). Accordingly, a series of such measurements had then to be averaged. The errors (or fluctuations) were attributed to turbulence or the occasional overlap of paper tracers.

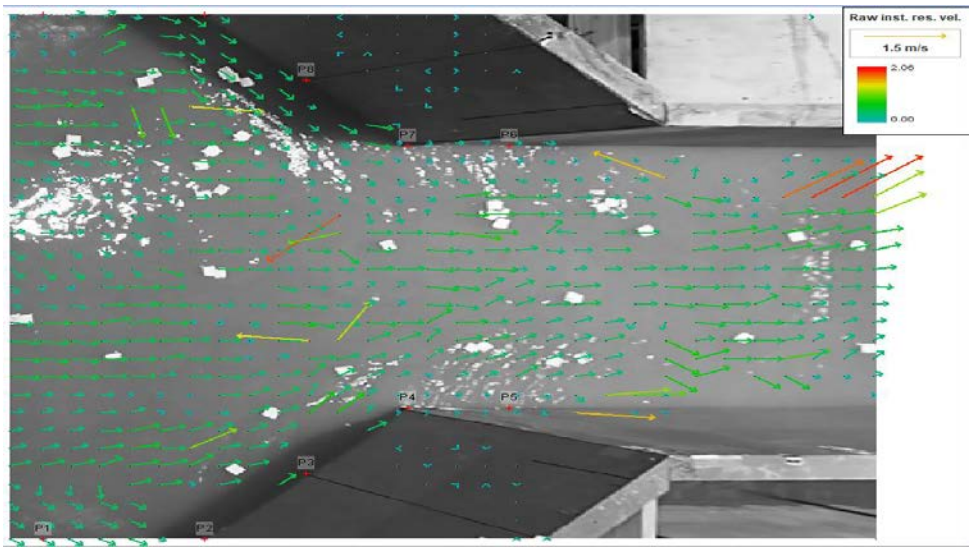

*Figure 3.24.*11 *The local velocity vectors (units are m/s) for the entrance to the open-channel contraction, including errant velocities, for B_2/B_1=0.5 and discharge= 0.23 m^3/s*

Figures 3.25 and 3.26 show the instantaneous vector velocities estimated using the Fudaa LSPIV for the Gross Dam experiment when the discharge was 0.347 m^3/s through the Vaqueros Dam model.

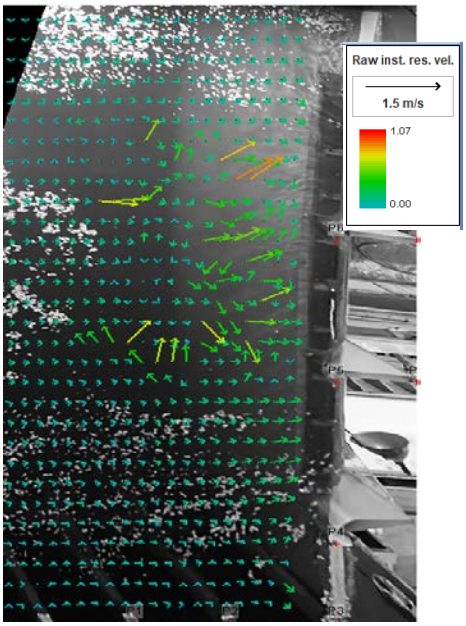

Figure 3.25. The local velocity vectors (units are m/s) for the spillway entrance of Gross Dam model, including errant velocities, for Q=0.347m^3/s

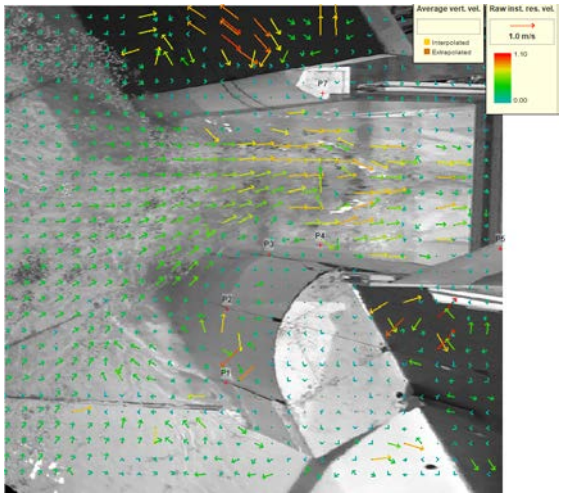

Figure 3.26. The local velocity vectors (units are m/s) for the spillway entrance of the Los Vaqueros Dam model, including errant velocities

After calculating the instantaneous velocities in each time step, it was necessary to define the velocity range to delete some unreal data (velocity magnitude or directions) and, thereby, to improve the accuracy of the results. Figures 3.27, 3.28, and 3.29 show the results obtained after applying the filtering for the 2.4-meter flume, the Gross Dam experiment, and the Vaqueros Dam model, respectively. Note the absence of any aberrational velocity vector in the flow field

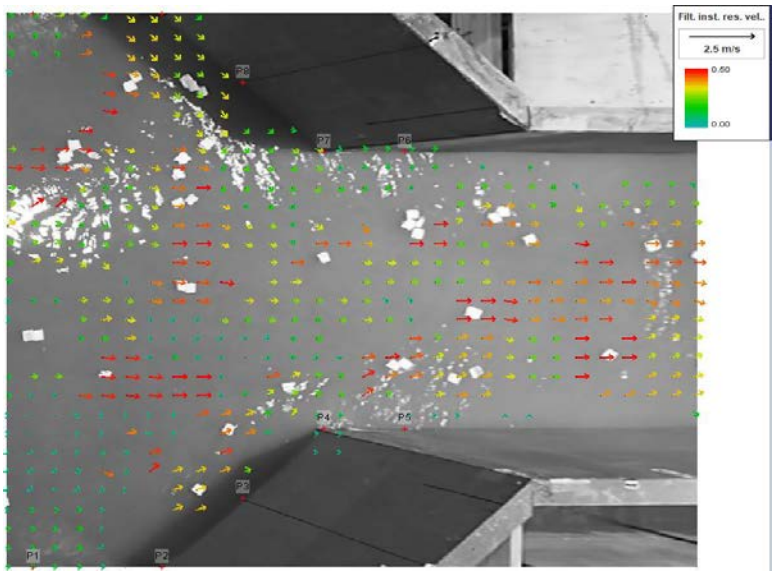

Figure 3.27. Instantaneous velocity vectors after applying the filter for B_2/B_1 = 0.5 and Q = 0.23 m^3/s (entrance to the open-channel contraction)

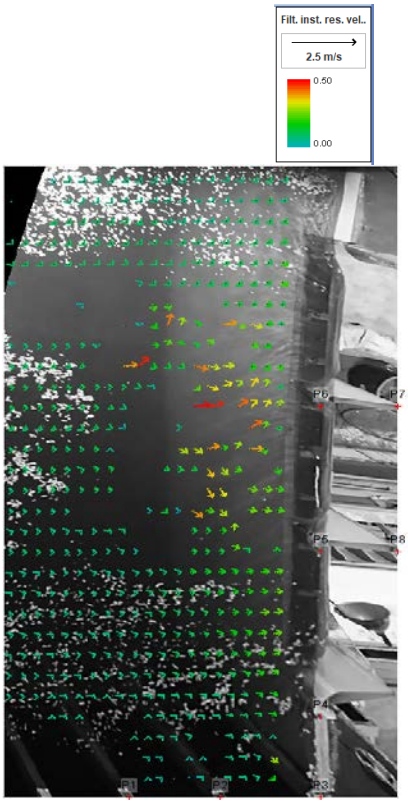

Figure 3.28. Instantaneous velocity vectors after applying the filter for the spillway entrance if the Gross Dam model; Q = 0.347m^3/s

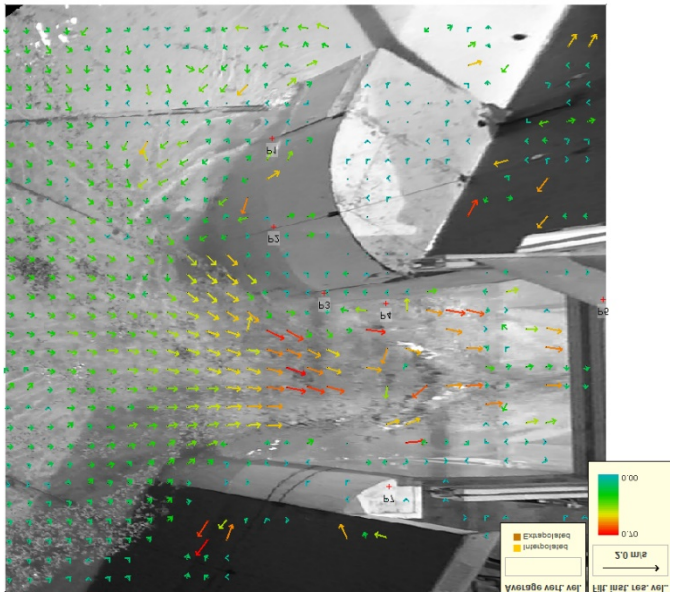

Figure 3.29. Instantaneous velocity vectors after applying the filter for the entrance of the Los Vaqueros Dam model; $Q = 0.17\ m^3/s$

In the next step, the LSPIV software was used to calculate the average values of the surface velocity vectors and prepare a contour map for average surface velocities. Figures 3.30 and 3.31, respectively, show the average surface velocity vectors' calculated values and give the velocity contour map for $B_2/B_1 = 0.5$ and a discharge, $Q = 0.23\ m^3/s$. Figures 3.32 and 3.33 present the calculated velocity vectors and velocity contour map for the Gross Dam model.

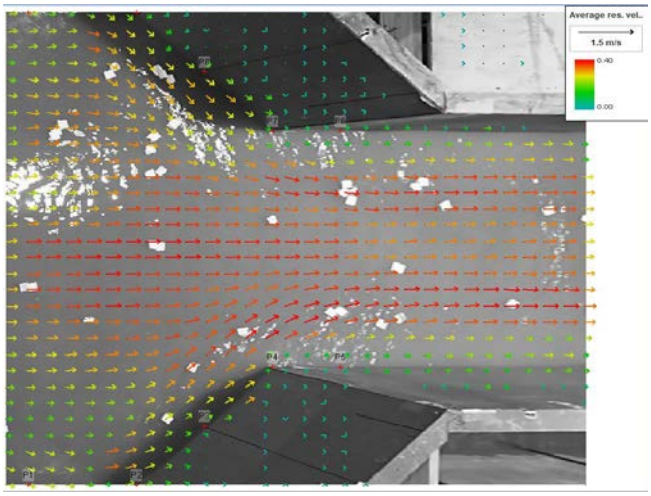

Figure 3.30. The average velocity vectors for $B_2/B_1 = 0.5$ and $Q = 0.23\ m^3/s$ (entrance to the open-channel contraction)

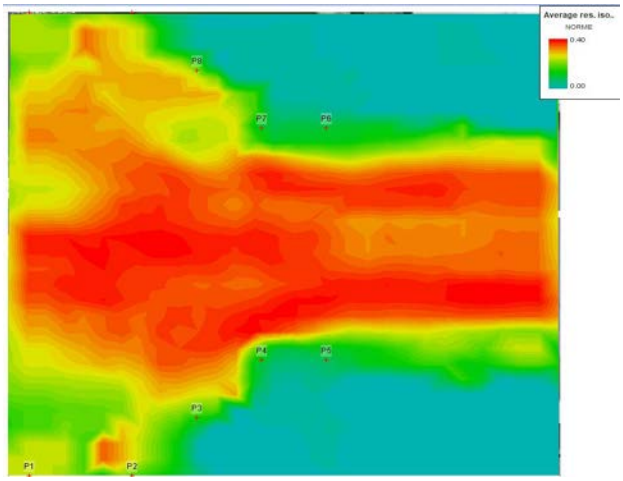

Figure 3.31. The velocity contour map for $B_2/B_1 = 0.5$ and $Q = 0.23\ m^3/s$. The benchmark locations are indicated (entrance to the open-channel contraction)

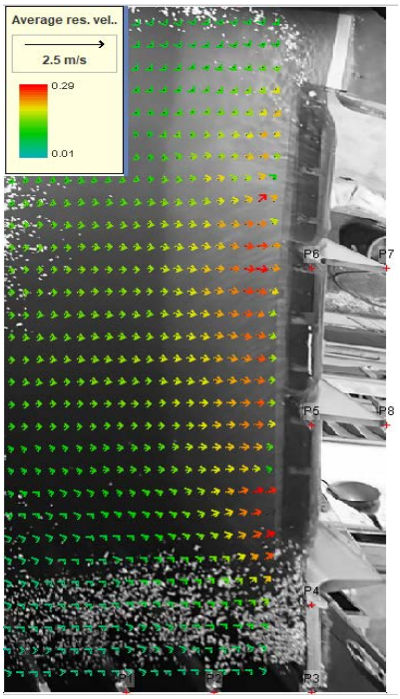

Figure 3.32. The average velocity vectors for the spillway of the Gross Dam model; Q = 0.347m^3/s.

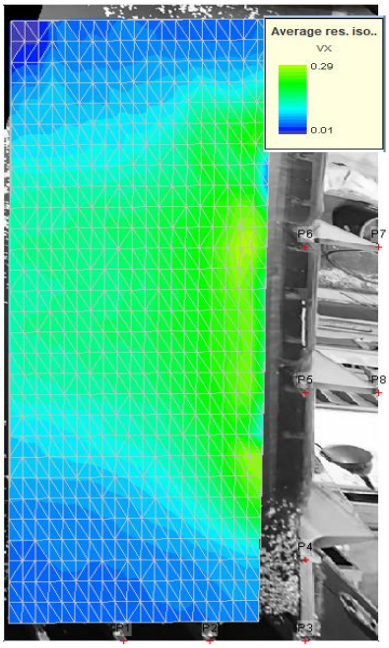

Figure 3.33. The velocity contour map for the entrance of the Gross Dam model; Q = 0.347m^3/s.

Figures 3.34 and 3.35 present the average velocity vectors and contour map when the discharge is 0.17 m^3/s, respectively.

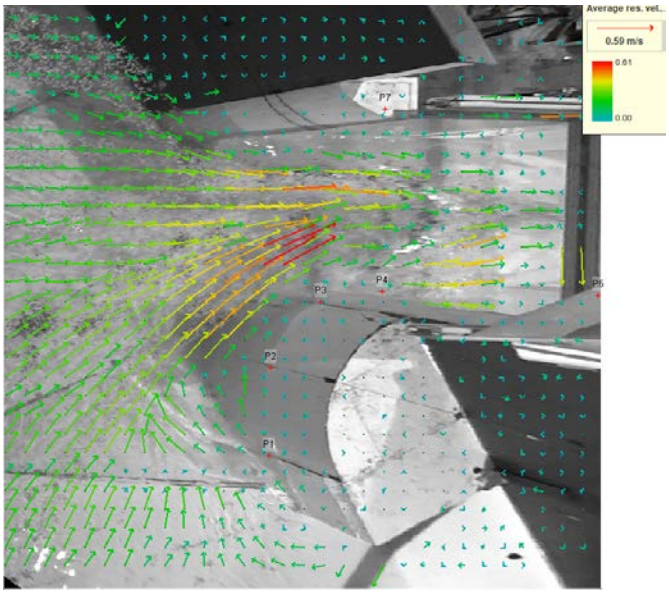

Figure 3.32. The average velocity vectors for the spillway entrance of the Vaqueros Dam model; Q = 0.17m^3/s.

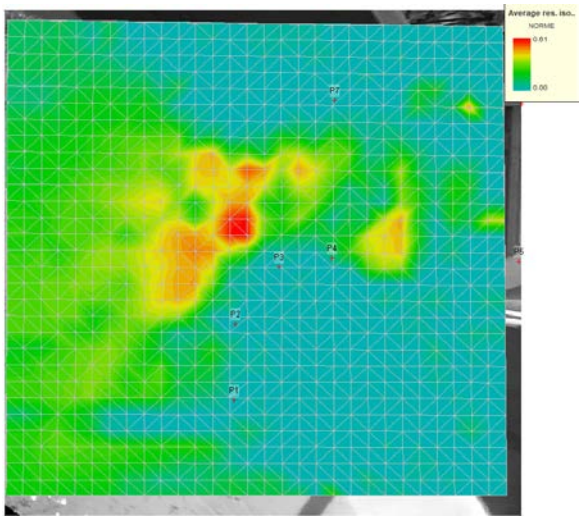

Figure 3.33. The velocity contour map for the spillway entrance of the Vaqueros Dam model; Q = 0.17m^3/s.

4. Results

In this section, to define the accuracy of results, following two terms were used:

- Acceptable: adequate, for the purpose of the study, to delineate the entire, water-surface flow field at the entrance.
- Unacceptable: not adequate, for the purpose of the study, to delineate the entire, water-surface flow field at the entrance. Usually, there were substantial gaps in the water-surface flow field.

4.1 The 2.4-meter Flume

The results comprise findings regarding the values of IA and the SA, and then the findings regarding the trend for flow contraction through the vena contracta formed in a contracted open channel. Figure 4.1 is an example of selected IA, SA, and their location when B_2/B_1=0.5.

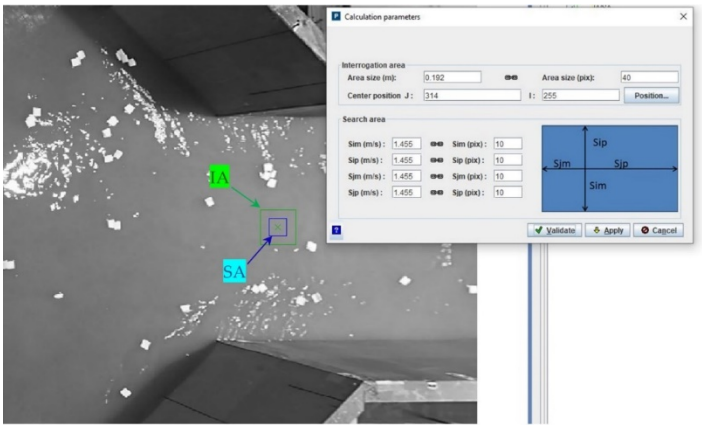

Figure 4.1. Delineation of the search area (SA) and the interrogation area (IA) (entrance to the open-channel contraction)

4.1.1 Interrogation Area and Search Area values

The results for different values of IA at the centerline of the flume (Line-D) are shown in Figure 4.2. In this plot, the black line indicates the measured velocities by ADV at the centerline. This plot demonstrates that the velocities measured by means of LSPIV, when IA is between 40 to 80 pixels, have the minimum range of errors between 1% to 5%, and the best value of IA is 80 pixels. Furthermore, it can be concluded that the IA range between 40 and 80 pixels still has an acceptable level of accuracy. Figure 4.3 shows the measured velocities in the vicinity of the centerline (line-C). Velocities calculated using LSPIV indicate that the precision is acceptable when IA is above 50 pixels, and it is insensitive to any change in IA values greater than 50 pixels. Also, it implies that the maximum errors occur at point C1, where the tracers enter the flow region. Figure 4.4 shows the measured velocities at line-B, thereby indicating that the measured velocities are insensitive to change in the value of IA, and smaller values of IA give a better result at regions where the velocity gradient is high.

Also, it can be concluded that the maximum value occurs where the tracers enter the flow region. Figure 4.5 depicts the velocities near the wall (Line-A). This plot reveals that the measured velocity vectors have the maximum accuracy when IA is within 30 and 90 pixels, and between this range, the results are insensitive to change of IA. Moreover, this plot shows that the measured velocities by LSPIV differ from ADV, and the level of error increases where particles reach the contraction. The possible reasons for the differences are the high-velocity gradient and tracer particles being close to the boundaries.

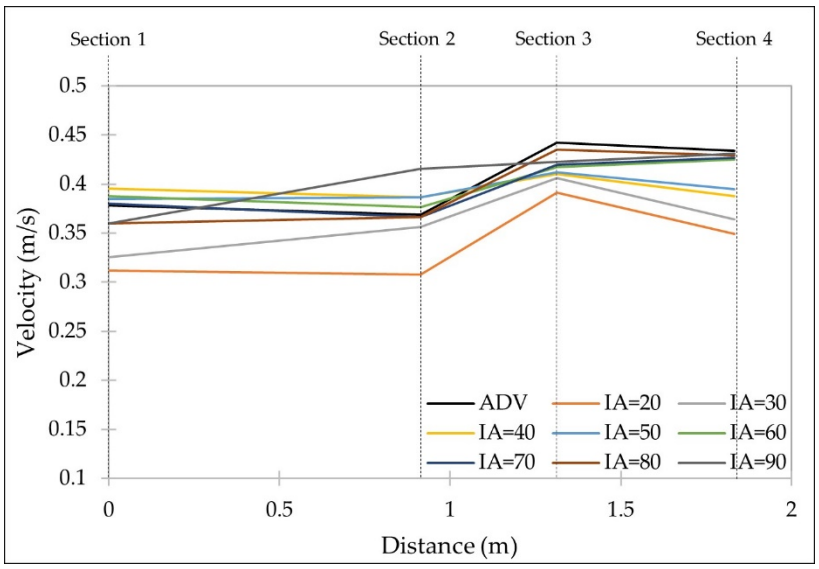

Figure 4.2 Measured Velocities obtained using LSPIV and ADV at Line-D (see Figure 3.20) (entrance to the open-channel contraction)

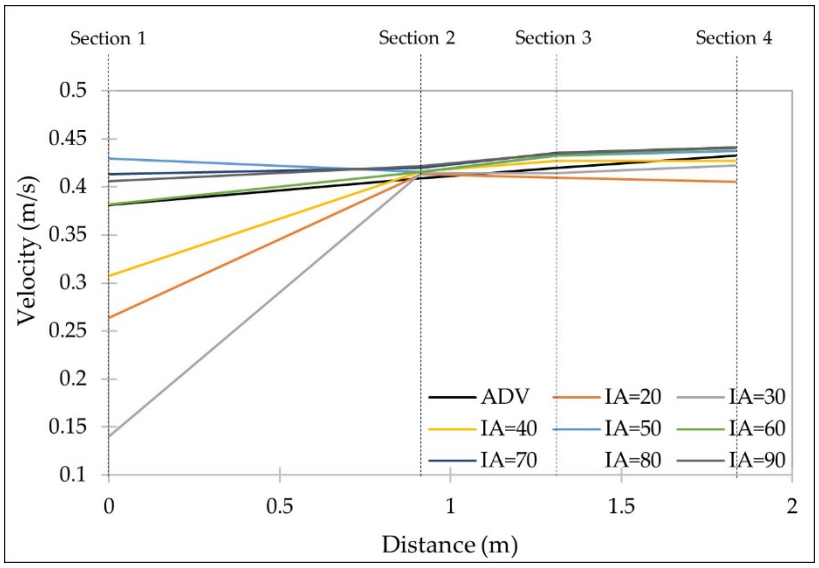

Figure 4.3. Measured Velocities obtained using LSPIV and ADV at Line-C (See Figure 3.20) (entrance to the open-channel contraction)

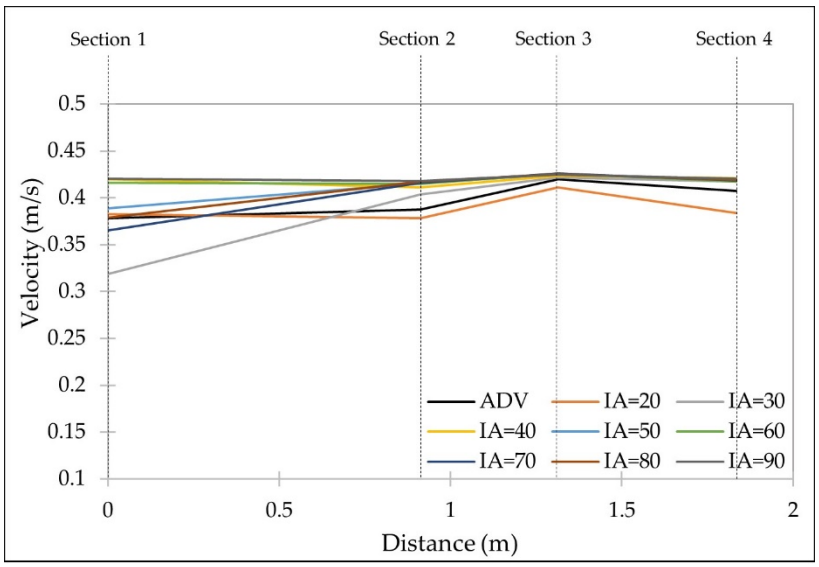

Figure 4.4. Measured velocities obtained using LSPIV and ADV at Line-B (See Figure 3.20) (entrance to the open-channel contraction)

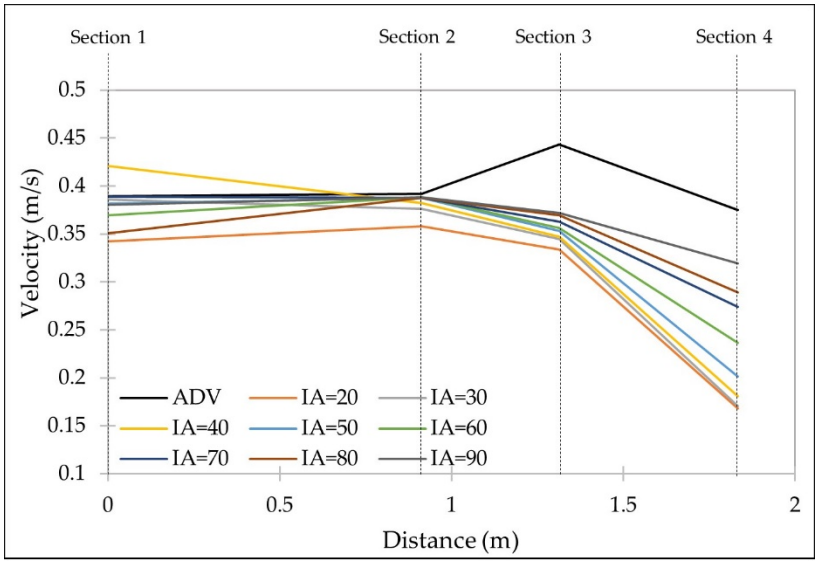

Figure 4.5. Measured velocities obtained using LSPIV and ADV at Line-A (See Figure 3.20) (entrance to the open-channel contraction)

The IA value was selected to be 80 pixels in the next step, and different SA values were set. The sensitivity of SA was investigated at the centerline (Line-D). Figure 4.6 represents the results for IA = 80 pixels and SA = 5, 10, 15 pixels. This plot indicates that the measured velocities by

LSPIV have an acceptable range of errors when SA's value is below 10 pixels. Furthermore, values of SA higher than 10 pixels have a significant increase in computational time.

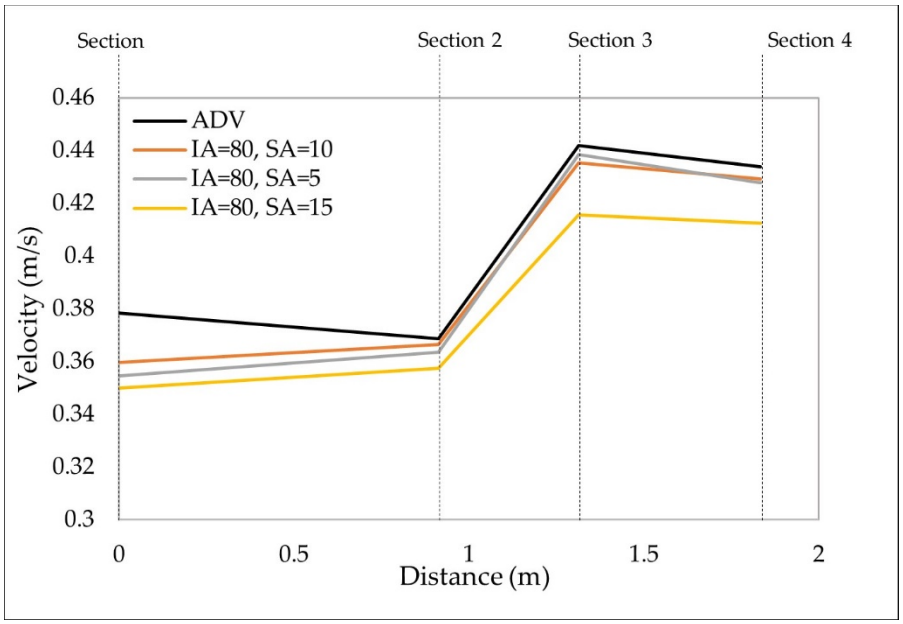

Figure 4.6. The sensitivity of measured velocities to SA at the centerline (Line-D) (entrance to the open-channel contraction)

4.1.2 Flow Mapping

The results presented in the previous section indicate that selecting IA to be between 40 to 80 pixels can accurately determine the velocity vectors and streamlines for lines B, C, and D, and precision is higher when IA is 80 pixels. For line A, when the flow reaches the contraction and near the walls, drawing the streamlines showed that LSPIV could precisely map the flow when IA is 60 pixels. For having a clear definition of the overall flow pattern, especially near the walls and contraction, IA and SA were selected at 60 and 10 pixels, respectively. This selection has an adequate precision for measuring velocities, and it can map the flow pattern precisely. The capability of flow mapping by LSPIV when IA is 80 and 60 pixels is compared in Figure 4.7. This

figure reflects some errors in drawing the streamlines at the tip of contraction when IA is equal to 80 pixels.

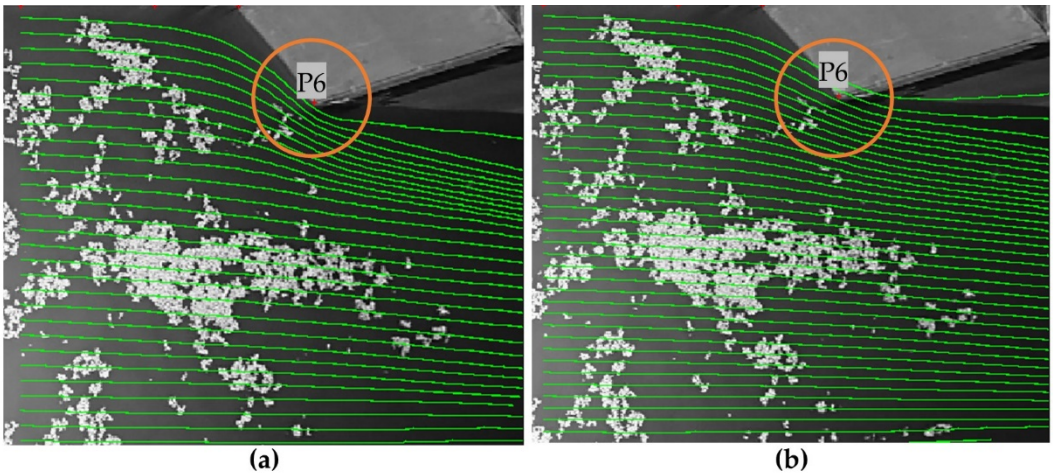

Figure 4.7. The surface flow field in the contraction entrance when B_2/B_1 = 0.75: (a) streamlines when IA=60 pixels; and, (b) streamlines when IA = 80 pixels.

With the IA and SA's selected values, the remaining 19 tests were conducted to plot the streamlines. The defined streamlines and the velocity vectors by LSPIV for the contraction ratio of 0.25, and the discharge of 0.064 m^3/s, are depicted in Figures 4.8 (a) and 4.8 (b), respectively. This figure shows that setting the LSPIV parameters to IA = 60 and SA = 10 aided accurate mapping of the flow pattern. Furthermore, the velocity vectors were drawn correctly in terms of magnitude and direction.

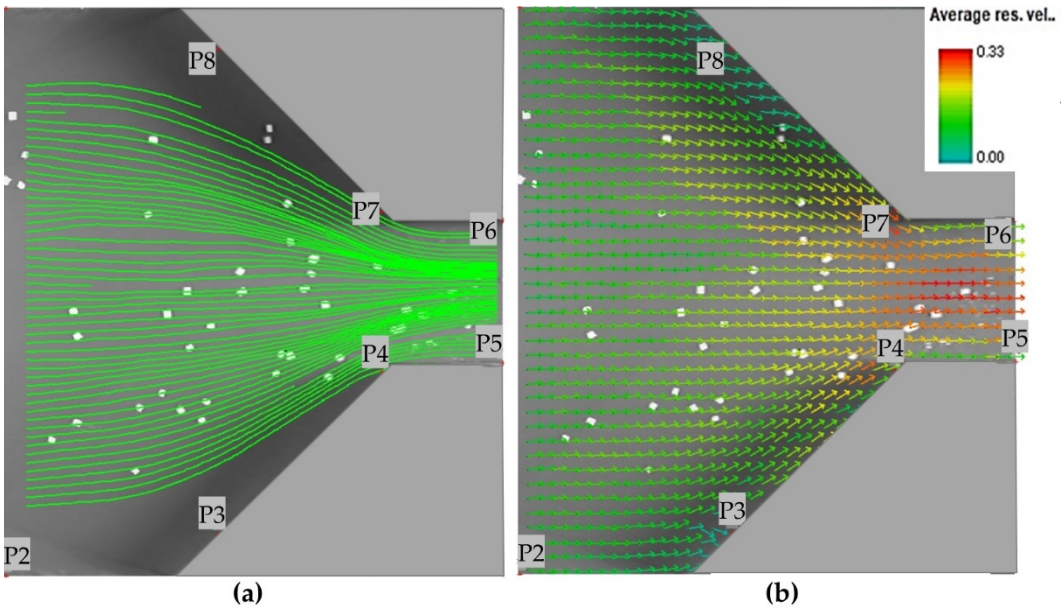

Figure 4.8. Views of streamlines: (a) streamlines; and, (b) velocity vectors for Q = 0.064 m^3/s and B_2/B_1 = 0.25; (entrance to the open-channel contraction)

Figures 4.9 and 4.10 illustrate the streamlines and velocity vectors for B_2/B_1 = 0.5 and 0.75 and when the discharges are 0.076 m^3/s and 0.128 m^3/s, respectively. These figures indicate that the selected parameters can adequately determine the flow pattern and velocity vectors for different contraction ratios.

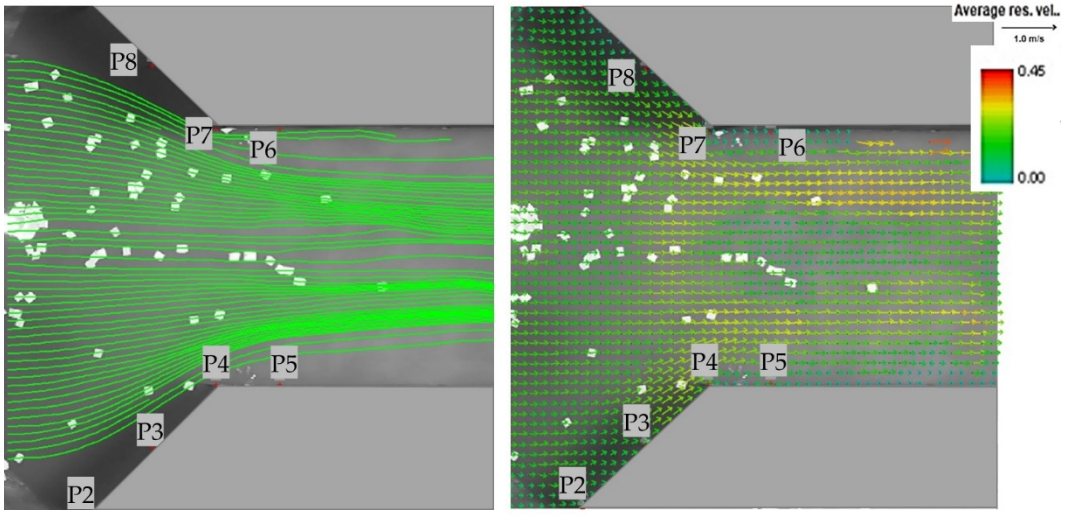

Figure 4.9. Views of streamlines:(a) streamlines; and, (b) velocity vectors for B2/B1 = 0.5 and Q = 0.23 m3/s; (entrance to the open-channel contraction)

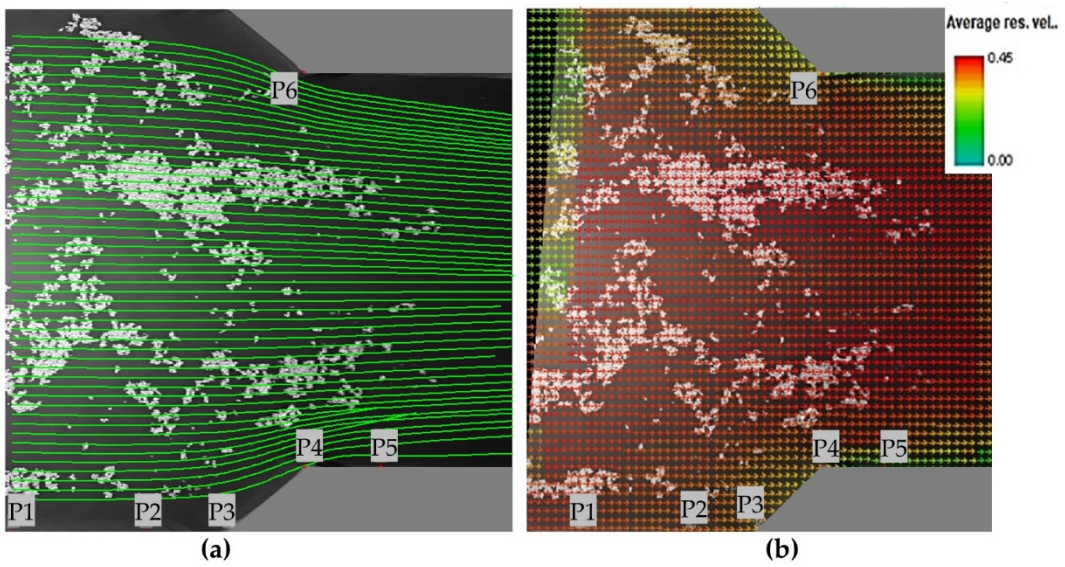

Figure 4.10. Views of streamlines: (a) streamlines; and, (b) velocity vectors for B2/B1 = 0.75 and Q = 0.138 m3/s; (entrance to the open-channel contraction)

4.1.3 Values of Vena-Contracta Width

The FUDAA Version 1.6.1 software enabled calculation of the streamlines in the flow field, which then were used for delineating the minimum top width of a vena contracta; i.e., where the contracta was narrowest. In this step, a straight line was drawn transverse across the flow to indicate the flow field from which streamlines were to be drawn. For the FUDAA software's present application, the straight line was drawn at the contraction's entrance cross-section. The defined line for B_1/B_2 = 0.5 and discharge = 0.23 m^3/s, and the corresponding streamlines are shown in Figures 4.11 and 4.12, respectively.

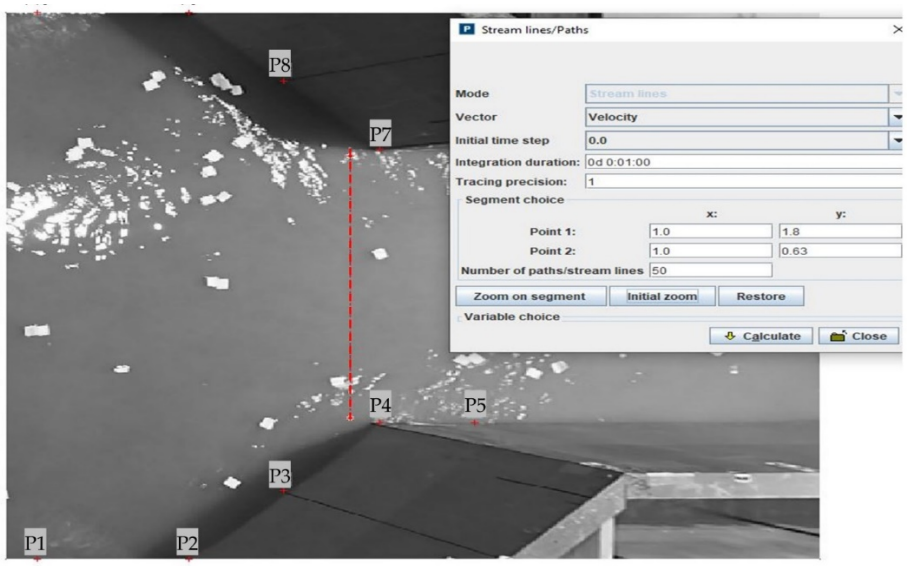

Figure 4.11. The defined transverse line as used for estimating the positions of the streamlines; (entrance to the open-channel contraction)

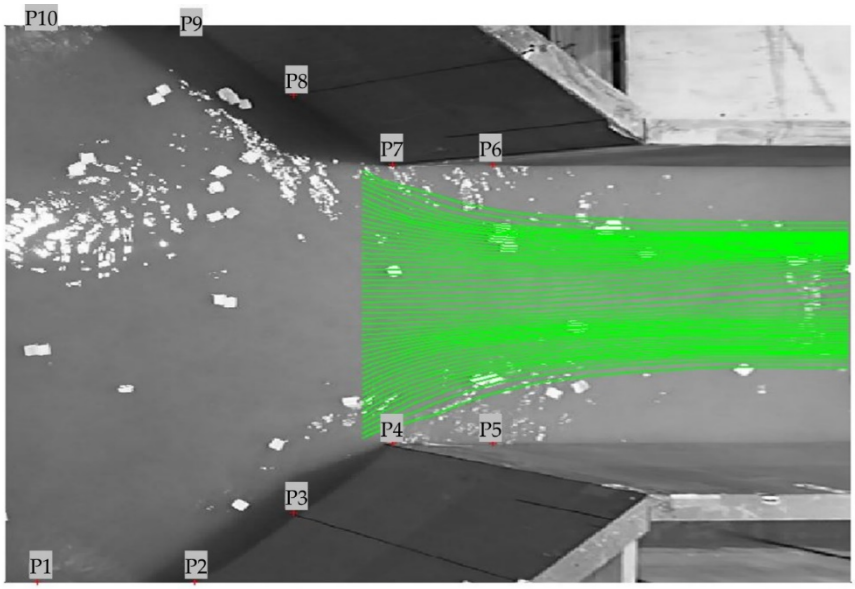

Figure 4.12. Estimated streamlines obtained for B_2/B_1 = 0.5 and discharge = 0.23 m^3/s; (entrance to the open-channel contraction)

The different contraction ratio values results, B_1/B_2, and discharges were then uploaded into an AutoCAD file. Later, all the images were scaled, and the vena contracta width, **B_2'**, was measured. To ensure clarity of the presentation, repeated here are the variables used in this process:

B_1 = the width of the approach channel

B_2 = the width of the contracted channel

B_2' = the minimum width (the width) of the vena contracta

V = velocity of uniform approach flow upstream of contraction

Y = depth of uniform approach flow upstream of contraction

g = gravity acceleration

Fr = Froude number of the uniform approach flow

Figure 4.13 is an illustrative example of the (minimum) vena contracta width estimated for $B_2/B_1 = 0.5$ and $Q = 0.23$ m^3/s. This figure shows the dimensions of the flow entering the contracted channel and the main dimensions measured using the LSPIV technique. Some other example results for the other contraction ratios and discharges are presented in Figures 4.14 and 4.15.

The LSPIV measurements for the ranges B_2/B_1 and τ_1/τ_c in the flume experiments were examined to estimate vena contracta coefficient $K_v = B_2'/B_2$ for the entrance configurations tested. The values obtained for K_v were plotted as the two curves depicted in Figure 4.16. Table 4.1 gives the measured vena contracta ratios estimated for all the experiments. The values were determined at the end of each experiment. As Figure 4.16 shows, they corresponded to equilibrium scour conditions within the contraction to aid scour estimation. Also, three values of K_v were estimated for the tight contraction, $B_2/B_1 = 0.25$, when the contracted channel's bed was fixed flat. Values of K_v also were determined for the initial conditions of runs with $B_2/B_1 = 0.25$. The trends in Figure 4.16 show that the measured top width of vena contracta decreases asymptotically as the abscissa term $(B_1/B_2 - 1)$Fr increases. This nondimensional term describes the narrowing of the vena contracta for increased approach-flow velocities expressed as $Fr = V/(gY)^{0.5}$. It cannot be bolstered by theoretical prediction because of the generation of oscillatory turbulence structures in flow separation regions, causing the vena-contracta to form. The lower curve in Figure 4.16 indicates that, before scour enlarging of the flow cross-sectional area, the vena-contracta width was less than after scour. The upper curve is the more useful for estimating bridge-waterway scour because scour equilibrium is based upon flow area at equilibrium scour depth.

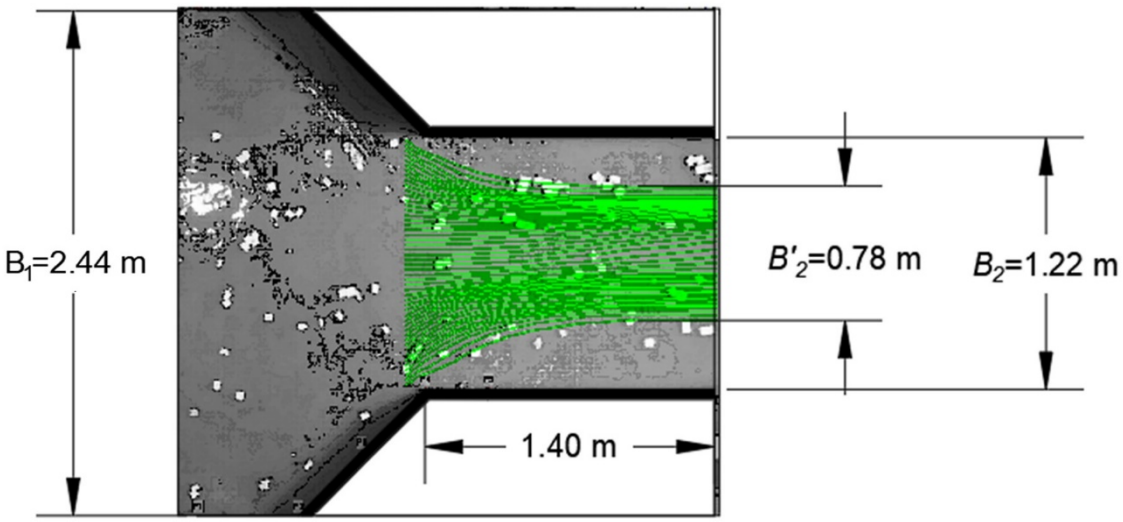

Figure 4.13. The measured value of vena contracta width B_2' obtained for experiment with B_2/B_1 = 0.5 and discharge of 0.23 m^3/s; (entrance to the open-channel contraction)

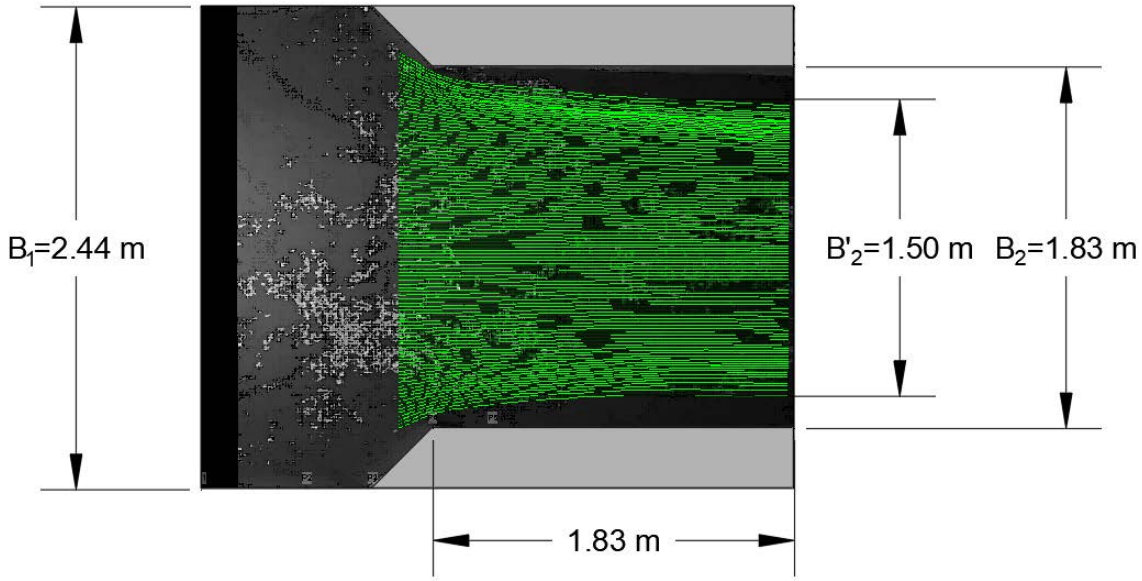

Figure 4.14. The measured value of vena contracta width B_2' obtained for experiment with B_2/B_1 = 0.75 and discharge of 0.099 m^3/s; (entrance to the open-channel contraction)

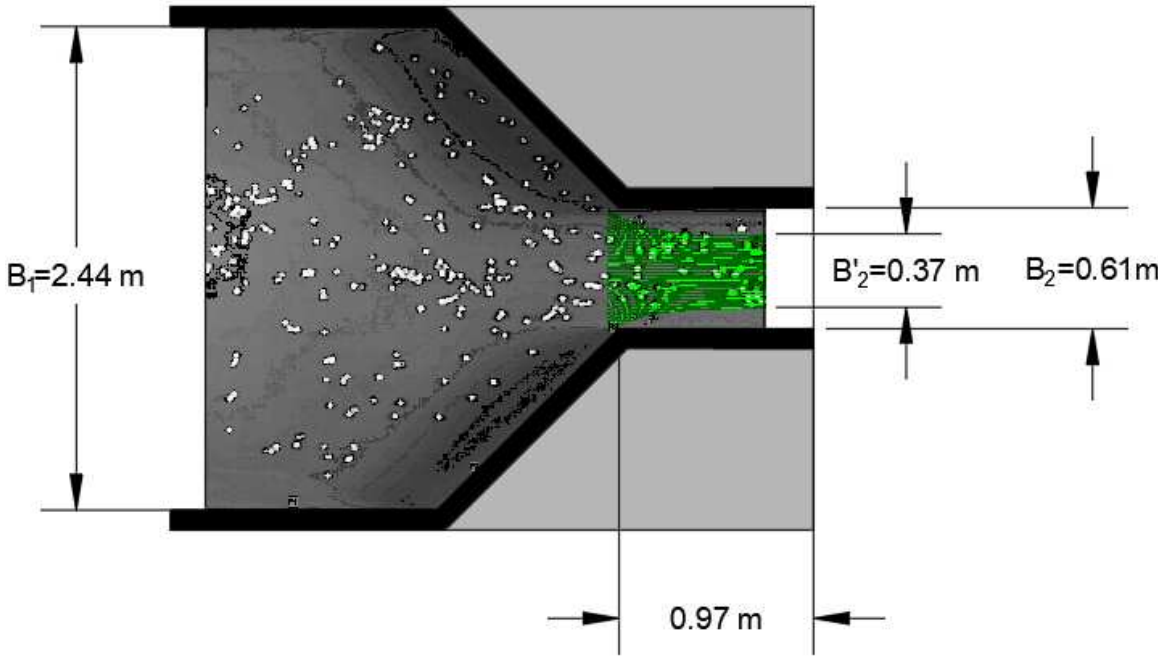

Figure 4.15. The measured value of vena contracta width B_2' obtained for experiment with B_2/B_1 = 0.25 and discharge 0.087 m^3/s; (entrance to the open-channel contraction)

Table 4-1. Summary of estimated vena contracta ratios and details for all experiments (entrance to the open-channel contraction)

Test Condition	**Contraction Ratio, B_2/B_1**	**Discharge, Q** (CMS)	B_2' (m)	(B_2'/B_2)	V (m/s)	Fr	(B_1/B_2-1) **Fr**
LB	0.75	0.190	1.52	0.83	0.44	0.332	0.109
LB	0.75	0.231	1.41	0.77	0.53	0.403	0.133
CW	0.75	0.111	1.50	0.82	0.26	0.194	0.064
LB	0.75	0.161	1.46	0.80	0.37	0.281	0.093
LB	0.75	0.138	1.44	0.79	0.32	0.241	0.079
LB	0.75	0.288	1.39	0.76	0.66	0.503	0.166
CW	0.75	0.099	1.61	0.88	0.23	0.173	0.057
CW	0.25	0.064	0.42	0.69	0.15	0.112	0.335
CW	0.25	0.087	0.37	0.61	0.20	0.152	0.456
LB	0.5	0.231	0.78	0.64	0.53	0.403	0.403
LB	0.5	0.161	0.81	0.66	0.37	0.281	0.281
LB	0.5	0.190	0.77	0.63	0.44	0.332	0.332
LB	0.5	0.138	0.83	0.68	0.32	0.241	0.241
CW	0.5	0.064	0.95	0.78	0.15	0.112	0.112
CW	0.5	0.076	0.88	0.72	0.17	0.133	0.133
CW	0.5	0.087	0.86	0.70	0.21	0.152	0.152
FB	0.25	0.064	0.27	0.44	0.15	0.112	0.335
FB	0.25	0.092	0.21	0.35	0.21	0.161	0.482
FB	0.25	0.076	0.23	0.37	0.17	0.133	0.398

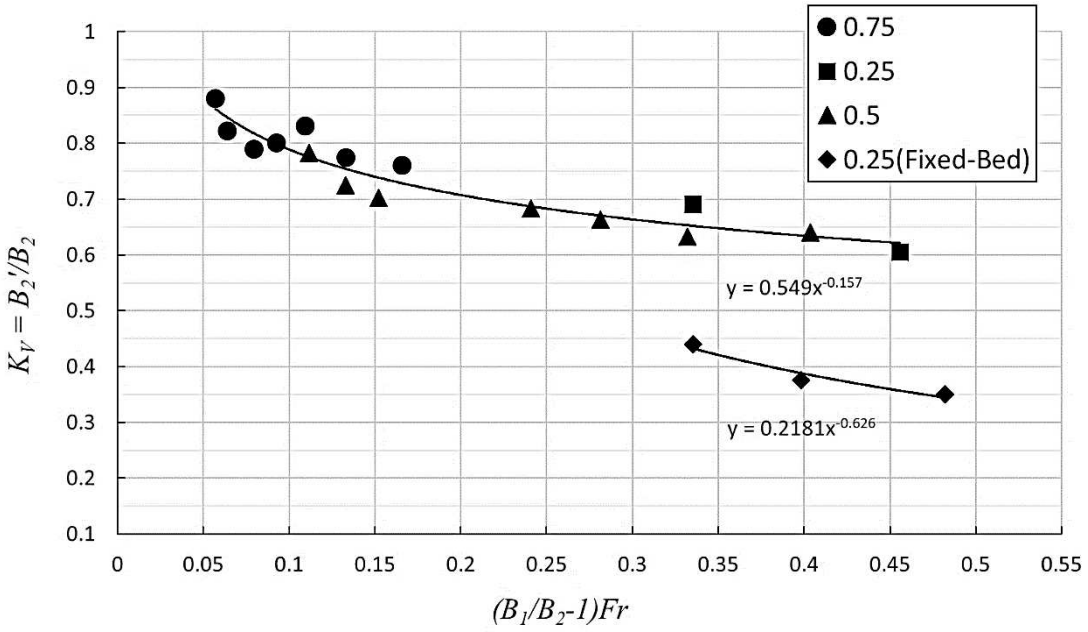

Figure 4.16. Values of vena-contracta coefficient, K_v, for a loose boundary channel with a 45˚ channel entrance. Two curves are shown: the fixed bed indicates the value of K_v before contraction-scour developed. Displayed in the legend box are the values of B_2/B_1; (entrance to the open-channel contraction)

4.2 Gross Dam

In the Gross Dam model, the lateral uniformity of flow distribution to and over the ogee crest was of interest, especially for evaluating the spillway's performance. Thus, to evaluate the capabilities of the dam model, the streamlines were mapped. As mentioned in the previous sections, the IA and SA were selected to be 60 and 10 pixels to map the flow, respectively. During the experiments, it turned out that using small tracers can map the flow pattern more precisely. Problems associated with the experiments were separation and a big gap between particles, which adversely affected the flow mapping. This happened due to having different approach lengths and flow directions through the weir. To solve this problem, it was devised to seed the head tank from three sides instead of seeding just from the center. The benefit of this seeding method was that,

with a proper timing between seedings, it can overcome problems due to different approach lengths. Figures 4.17 and 4.18 show the measured velocity vectors and the velocity contour map, respectively.

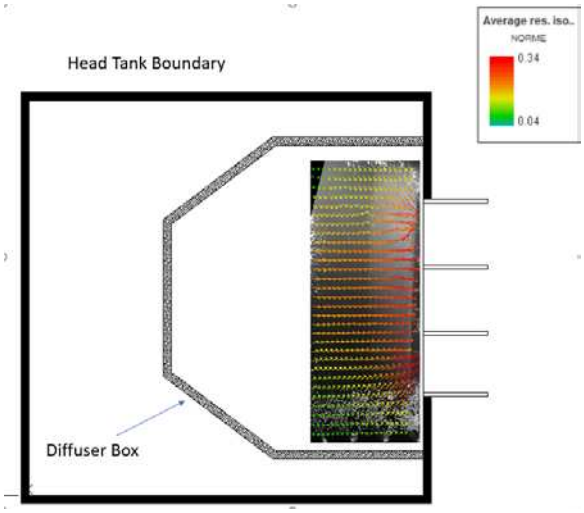

Figure 4.17. The measured velocity vectors for the entrance to the spillway of the Gross Dam model; Q=0.347m^3/s

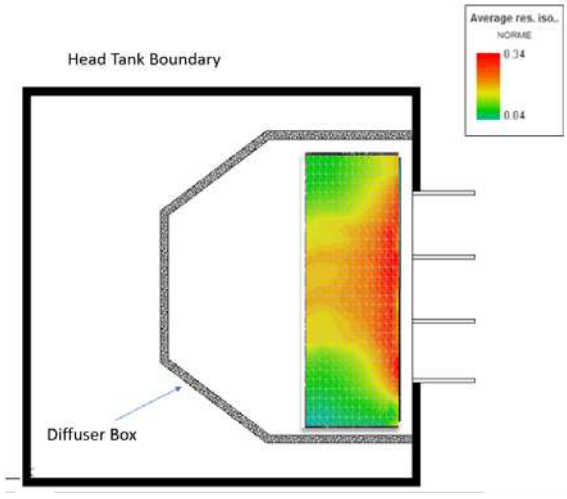

Figure 4.18. The velocity contour map for the Gross Dam model; Q=0.347m^3/s

One of the factors needed to design and operate the Gross Dam model was the uniformity of flow through the weir, especially from corners. To check the capability of the LSPIV method for determining the flow pattern, streamlines were drawn in the center and one corner. The reason was that FUDAA LSPIV software can map the flow pattern from a straight line, which makes it impossible to map the whole flow pattern in the head tank. Therefore, for this specific application, the flow region was seen from the corner and center. Figures 4.19 and 4.20 show the calculated streamlines at the center and corner of the head tank, respectively. These figures indicate that LSPIV is a robust technique for flow mapping in the head tank where the flow is not wavy, and there is not flow motion in Z direction.

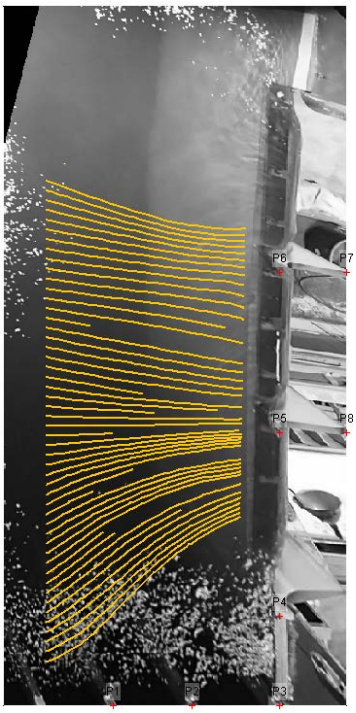

Figure 4.19. Streamlines at the center of head tank for the Gross Dam model;Q = 0.347 m^3/s

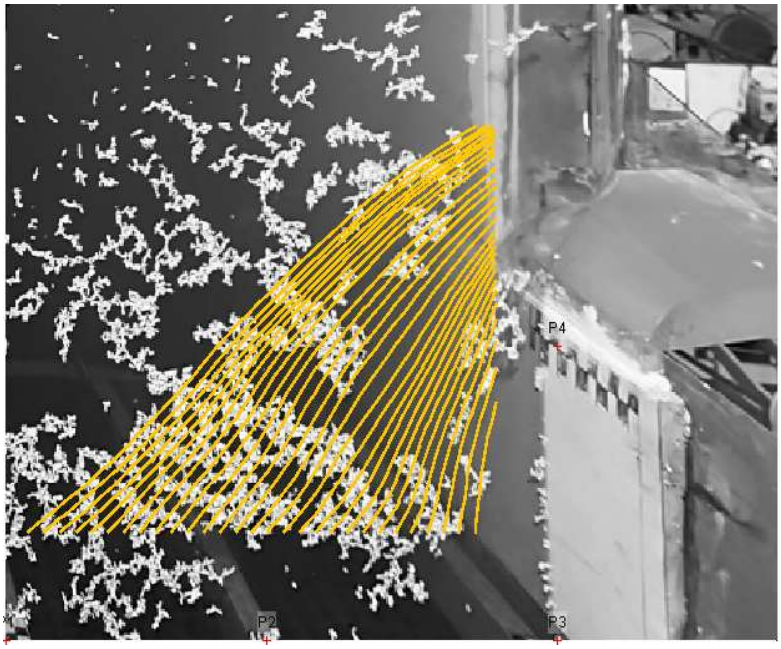

Figure 4. 20. Streamlines at the corner of head tank for the Gross Dam model; Q = 0.347 m^3/s

4.3 Los Vaqueros Dam

In the model of the spillway for Los Vaqueros Dam, the lateral flow uniformity and the flow separation zones were of interest. To assess the capability of the model, the streamlines were calculated. For the seeding part, based on the finding from the previous section, fine particles were used to have better coverage over the head tank. The IA and SA were selected to be 60 and 10 pixels, respectively. Figures 4.21 shows the streamlines in the head tank when the discharge was 0.17 m^3/s.

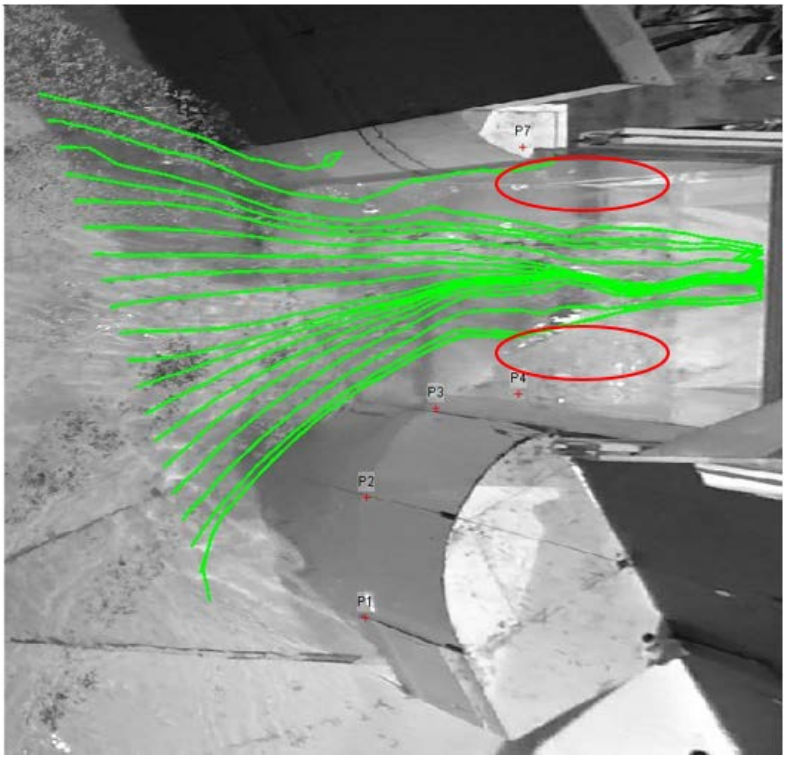

Figure 4. 21. Streamlines in the head tank for the spillway entrance for the Los Vaqueros Dam model; $Q = 0.17\ m^3/s$

The regions marked with red color in this picture indicate the flow separation in this model. This figure shows that the flow has a proper uniformity in the head tank, although the streamlines in the outlet faces flow separation in both sides.

5. Conclusions and Recommendations

5.1 Conclusions

Besides the limitations inherent in selecting suitable values of SA and IA (as discussed above), LSPIV was found to become less accurate for estimating velocities of flow in regions where the flow developed waviness, thereby causing flow to have vertical components of velocity at the water surface, though LSPIV still was sufficiently accurate for the purpose of estimating the minimum width of a vena contracta. The vertical fluctuations of flow decreased the estimated magnitudes of velocity by lengthening the flow path by including an upward and downward component. This limit was noticeable when the contraction ratio $B_2/B_1 = 0.25$, in which standing waves formed. Though the estimated width of vena contracta was sufficient (the estimated width agreed with observations by eye), the velocities were less than values estimated from the velocity profile obtained using ADV.

Another limitation documented elsewhere is that the tracer particles must be suitably small to delineate flow structures visible on the water surface. This limitation was addressed in the study and led to selecting the tracer size used, as mentioned above. Under these conditions, the turbulence from the separation zones at the entrance corners caused the vena-contracta boundaries to oscillate. Small standing waves developed from the entrance corners led the tracer particles to move up and down when passing into the contracted channel. Therefore, the use of LSPIV in conditions where the water-surface was wavy did not result in reliable estimates of velocity at the flow surface. However, the estimates of B_2' were considered sufficiently useful to complete the trends shown in Figure 4.16.

The study led to the following main conclusions:

1. LSPIV is a useful and readily applicable way to illuminate flow patterns at water-surfaces, and indeed to obtain estimates of flow velocities at the water surface. Such water surfaces must be planar, however, if flow velocities are to be assessed. The present study focused on LSPIV use for estimating the narrowest width of a vena contracta formed in an open-channel contraction, and particularly on the influences consequent to selecting the Search Area (SA) and Interrogation Area (IA) when applying LSPIV. These foci are missing from the literature on LSPIV use.
2. Values of SA should be between 5 and 10 pixels. Also, SA is insensitive to values above 10 pixels. However, values higher than ten pixels increase the computational time significantly.
3. The IA values should exceed 80 pixels to give acceptable accuracy (for the present study) when the region is straight, with no contraction. The level of accuracy declines at boundaries and when the velocity gradient is high. When the velocity gradient is high and the flow faces a contraction, IA = 60 gives a better precision in terms of magnitude and mapping the streamlines. Results from the IA investigations reveal some errors where the flow enters the interest area. To overcome this limitation, it is recommended that the grid lines at the entrance be extended to increase the level of accuracy in the area of interest.
4. The reach the maximum accuracy obtainable using LSPIV, this study suggests that researchers should consider the flow conditions to select appropriate SA and IA values. When finding the velocity magnitude is of interest with a low level of velocity gradient, IA

= 80 pixels, and SA = 10 can be used. When the flow is wavy, and the flow mapping is essential, IA = 40-60, and SA = 10 can be a convenient choice for the LSPIV parameters.

5. LSPIV showed that the minimum width of the vena contracta in an open-channel contraction conformed to the curves shown in Figure 4.16. However, its use still required judgment for the higher discharges through the smallest value of B_1/B_2 used (0.25). The values of k_V were substantial and decreased as the value of $(B_1/B_2 - 1)\ Fr$ increased.

5.2 Recommendations for further research

1. Determine the effect of vertical motion (waves or a component of flow moving in vertical plane) on the accuracy of the LSPIV method.
2. Figure 4.16 needs further development for other entrance shapes, fixed bed versus loose bed, and contraction ratios.
3. Determine how the vena-contracta varies over the full depth of flow, not just at the water surface.

6. References

1. Fujita, I.; Muste, M.; Kruger, A. Large-scale particle image velocimetry for flow analysis in hydraulic engineering applications. J Hydraul Res **1998**, 36, 397-414. DOI: 10.1080/00221689809498626.
2. Coz, J. L., Hauet, A., Pierrefeu, G., Dramais, G. & Camenen, B. Performance of image-based velocimetry (LSPIV) applied to flash-flood discharge measurements in Mediterranean rivers. J. Hydrol. **2010**, 394, 42–52.
3. Guillén, N. F., Patalano, A., García, C. M. & Bertoni, J. C. Use of LSPIV in assessing urban flash flood vulnerability. Nat. Hazards **2017**, 87, 383–394.
4. Al-mamari, M., Kantoush, S., Kobayashi, S., Sumi, T. & Saber, M. Real-Time Measurement of Flash-Flood in a Wadi Area by LSPIV and STIV. Hydrology **2019**, 6, 27.
5. Dramais, G., Le Coz, J., Camenen, B. & Hauet, A. Advantages of a mobile LSPIV method for measuring flood discharges and improving stage-discharge curves. J. Hydro-Environment Res., **2011**, 5, 301–312.
6. Tsubaki, R., Fujita, I. & Tsutsumi, S. Measurement of the flood discharge of a small-sized river using an existing digital video recording system. J. Hydro-Environment Res., **2011**, 5, 313–321.
7. Lewis, Q. W., Lindroth, E. M. & Rhoads, B. L. Integrating unmanned aerial systems and LSPIV for rapid, cost-effective stream gauging. J. Hydrol.,**2018**, 560, 230–246.
8. Bieri, M., Jenzer, J., Kantoush, S. A. & Boillat, J.-L. Large scale particle image velocimetry applications for complex free surface flows in river and dam engineering. Proc. 33rd IAHR Congr. Vancouver, Canada 604–611, 2009.
9. Fujita, I. & Aya, S. Refinement of LSPIV technique for monitoring river surface flows. Water Resour. **2000**, 1–9.
10. Harpold, A. A., Mostaghimi, S., Vlachos, P. P., Brannan, K. & Dillaha, T. Stream discharge measurement using a large-scale particle image velocimetry (lspiv) prototype. American Society of Agricultural and Biological Engineers **2006**, vol. 49 1791–1805.
11. Theule, J. I., Crema, S., Marchi, L., Cavalli, M. & Comiti, F. Exploiting LSPIV to assess debris-flow velocities in the field. Nat. Hazards Earth Syst. Sci. 2018. doi:10.5194/nhess-18-1-2018.
12. Sturm, Terry W. Open Channel Hydraulics. Boston: McGraw-Hill, 2001. Print.

13. Jodeau, M.; Hauet,A.; Coz, J. L. E.; Bercovitz, Y.; Lebert, F.; Edf, D. T. G.; Hhly, U. R. Laboratory and field LSPIV measurements of flow velocities using Fudaa-LSPIV, a free user-friendly software. Proc. 1st Int. Symp. Exhib. Hydro-Environment Sensors Softw. - HydroSenSoft, no. March, pp. 82–86, 2017.
14. Aberle, J.; Rennie, C.D.; Admiraal, D.M.; Muste, M. Experimental hydraulics: methods, instrumentation, data processing and management, Volume II; Taylor & Francis Group: London, UK, 2017; pp. 35-193. ISBN:978-1-138-03815-8.
15. Meselhe, E.A.; Peeva, T.; Muste, M. Large scale particle Image Velocimetry for low velocity and shallow water flows. J Hydraul Eng 2004, 130(9), 937-940. DOI: 10.1061/(ASCE)0733-9429(2004)130:9(937).
16. Chen, K. Application of Large-Scale Particle Image Velocimetry at the hydraulics laboratory of Colorado State University. M.S, Colorado State University, 2018.
17. Wahl, T. L. Refined Energy Correction for Calibration of Submerged Radial Gates. J. Hydraul. Eng. 2005 doi:10.1061/(asce)0733-9429(2005)131:6(457).
18. Epple, P., Steppert, M., Malcherek, A. & Fritsche, M. Theoretical and numerical analysis of the pressure distribution and discharge velocity in flows under inclined sluice gates. in ASME-JSME-KSME 2019 8th Joint Fluids Engineering Conference, AJKFluids 2019. doi:10.1115/AJKFluids2019-5020.
19. Hajimirzaie, S. M. & González-Castro, J. A. A New Energy-Based Rating Algorithm for Controlled Submerged Flow at Gated Spillways. in World Environmental And Water Resources Congress 2016: Hydraulics and Waterways and Hydro-Climate/Climate Change - Papers from Sessions of the Proceedings of the 2016 World Environmental and Water Resources Congress. doi:10.1061/9780784479872.003.
20. Thompson, D. M., Nelson, J. M. & Wohl, E. E. Interactions between pool geometry and hydraulics. Water Resoure Res. 1998. doi:10.1029/1998WR900004.
21. The use of a vertical pipe as an overflow for a large tank. Proc. R. Soc. London. Ser. A. Math. Phys. Sci. 1938. doi:10.1098/rspa.1938.0171.
22. Hager, W. H. Supercritical Flow in Channel Junctions. J. Hydraul. Eng. 1989. doi:10.1061/(asce)0733-9429(1989)115:5(595).
23. Hsu, C.-C., Wu, F.-S. & Lee, W.-J. Flow at 90° Equal-Width Open-Channel Junction. J. Hydraul. Eng. 1998 doi:10.1061/(asce)0733-9429(1998)124:2(186).

24. Schindfessel, L., Creëlle, S. & De Mulder, T. Flow patterns in an open channel confluence with increasingly dominant tributary inflow. Water (Switzerland) 2015. doi:10.3390/w7094724.
25. Sturm, Terry W. Open Channel Hydraulics. Boston: McGraw-Hill, 2001. Print
26. Sutarto, T.E. Application of Large-Scale Particle Image Velocimetry (LSPIV) to identify flow pattern in a channel. Procedia Eng 2015, 125, 213-219. DOI: 10.1016/j.proeng.2015.11.031.
27. Genc, O.; Ardıçlıoğlu, M.; Ağıralioğlu, N. Calculation of mean velocity and discharge using water surface velocity in small streams. Flow Meas. Instrum 2015, 41, 115-120. DOI: 10.1016/j.flowmeasinst.2014.10.013.
28. Fakhri, A.; Ettema, R.; Aliyari, F.; Nowroozpour, A. Large-Scale Particle Image Velocimetry for Estimating Vena-Contracta Width for Flow in Contracted Open Channels. Water 2021, 13, 31. https://doi.org/10.3390/w13010031.